

IMPLEMENTATION OF ENVELOPE TRACKING FOR RF SOLID STATE AMPLIFIERS

By

Thomas Leigh Larter

A THESIS

Submitted to  
Michigan State University  
in partial fulfillment of the requirements  
for the degree of

Electrical Engineering – Master of Science

2015

## ABSTRACT

### IMPLEMENTATION OF ENVELOPE TRACKING FOR RF SOLID STATE AMPLIFIERS

By

Thomas Leigh Larter

The Facility for Rare Isotope Beams (FRIB) is currently in its development stages at Michigan State University. The facility uses a large linear accelerator system to accelerate ionized particles which are then collided with other particles in the hopes of finding rare isotopes of elements. This accelerating action depends on several systems to function, with one of the major systems being superconducting cavity structures. These cavities are driven by high-power RF amplifiers which account for a large portion of the accelerator's power consumption. It is important to maximize the efficiency of these amplifiers in order to keep energy costs for the facility low.

One of the ways to increase efficiency is to choose an amplifier topology that is highly efficient. A study was done for FRIB testing the prospect of using amplifiers with the envelope tracking (ET) topology. An amplifier's efficiency relies on its output power and the power supplied to it, which are in turn directly related to the output signal voltage and supply rail voltage. In an ET RF amplifier, the supply voltage is made to closely follow the envelope of the output signal voltage. This tracking action allows the RF amplifier to operate with much improved efficiency at low power levels and nearly constant efficiency at high power levels.

The ET tests performed for FRIB attempted to verify the validity of ET efficiency gains for RF amplifiers. These tests included the characterization of an RF amplifier, development and verification of an ET control algorithm, and implementation of an ET test bench using FRIB equipment. These tests should attest to the purported increase in efficiency possible with ET and prove that the power consumption budget for the FRIB will benefit from the use of such amplifiers.

*To my parents, David and Ginger.*

## ACKNOWLEDGEMENTS

The author would like to thank Dan Morris and Nathan Usher for their assistance in this research.

## TABLE OF CONTENTS

LIST OF TABLES .....	vi
LIST OF FIGURES .....	vii
CHAPTER 1: INTRODUCTION .....	1
1.1 Rare Isotopes.....	1
1.2 Superconducting Cavities .....	3
1.3 Envelope Tracking and Energy Savings .....	8
1.4 Thesis Layout .....	9
CHAPTER 2: ENVELOPE TRACKING AMPLIFIERS .....	10
2.1 Classic RF Power Amplifier Design.....	10
2.2 Envelope Tracking.....	15
CHAPTER 3: CHARACTERIZING THE POWER AMPLIFIER.....	20
3.1 Characterization Test Setup.....	20
3.2 Characterization Test Results .....	24
CHAPTER 4: CONTROL ALGORITHM DEVELOPMENT.....	29
4.1 Test Bench Setup.....	29
4.2 ET Control Algorithm Development.....	31
CHAPTER 5: ET EXPERIMENTS WITHOUT MICROPHONICS.....	35
5.1 Experiment Test Setup .....	35
5.2 Experimental Results .....	37
CHAPTER 6: ET EXPERIMENTS WITH MICROPHONICS .....	43
6.1 Experiment Test Setup .....	43
6.2 Experimental Results .....	44
6.3 Issues with Experimental Setup.....	50
CHAPTER 7: CONCLUSION .....	52
7.1 Practical Considerations for ET .....	54
7.2 Future Work .....	55
APPENDIX .....	58
BIBLIOGRAPHY .....	72

LIST OF TABLES

Table 1-1 Projected power usage for RF amplifiers on the beamline ..... 8

Table 1-2 Projected energy cost savings for increased efficiency ..... 9

Table 4-1 Characterization data used in ET control algorithm creation ..... 32

Table 6-1 Comparison of efficiency between Class A and ET ..... 48

Table 6-2 Predicted average efficiency gains for PDF overlays ..... 49

## LIST OF FIGURES

Figure 1-1 Chart of expected FRIB isotope production.....	2
Figure 1-2 Layout of the FRIB accelerator.....	3
Figure 1-3 Cutaway view of cavities used on beamline.....	3
Figure 1-4 Variance of cavity response due to changes in cavity dimension .....	4
Figure 1-5 Cavity drive block diagram.....	5
Figure 1-6 Example of RF power modulation used to counteract cavity detuning from microphonics.....	6
Figure 1-7 Example of probability density function for cavity-drive power .....	7
Figure 2-1 Block diagram for static-supply amplifier .....	10
Figure 2-2 MOSFET output characteristics .....	11
Figure 2-3 Gain compression for a RF amplifier.....	12
Figure 2-4 Comparison of drain voltage to rail voltage for classical amplifiers.....	13
Figure 2-5 Variance of efficiency and gain with respect to output power for a constant rail voltage .....	14
Figure 2-6 Block diagram for ET amplifier.....	15
Figure 2-7 Efficiency and gain characteristics for an amplifier with various rail voltages and with ET.....	16
Figure 2-8 Comparison of drain voltage to rail voltage for ET amplifier at modulation threshold .....	17
Figure 2-9 Comparison of drain voltage to rail voltage for ET amplifier in full saturation .....	18
Figure 3-1 Block diagram for characterization tests .....	20
Figure 3-2 Experiment setup for characterization tests .....	21
Figure 3-3 Broadcast Concepts 55-88MHz 12W VHF TV model pallet amplifier.....	22
Figure 3-4 Directional coupler forward coupling factor vs. frequency.....	23
Figure 3-5 Measured pallet amplifier gain vs. input power for various supply voltages.....	24
Figure 3-6 Measured pallet amplifier gain vs. output power for various supply voltages .....	25

Figure 3-7 Measured pallet amplifier THD vs. Output Power.....	26
Figure 3-8 Measured pallet efficiency vs. output power .....	27
Figure 4-1 ET experiment setup block diagram .....	30
Figure 4-2 Efficiency data points chosen for ET algorithm .....	33
Figure 4-3 Gain data points chosen for ET algorithm .....	33
Figure 4-4 ET control algorithm derived from LLRF generated signal amplitude and desired rail voltage	34
Figure 5-1 Flowchart for live efficiency measurement script .....	36
Figure 5-2 Comparison of proposed ET control algorithm and measured performance .....	37
Figure 5-3 Comparison of measured ET and Class A performance.....	38
Figure 5-4 Efficiency difference between measured ET and Class A performance .....	39
Figure 5-5 Points of comparison chosen for real-time analysis.....	40
Figure 5-6 Real-time measurement of efficiency for ET and Class A, first comparison.....	41
Figure 5-7 Real-time measurement of efficiency for ET and Class A, second comparison.....	41
Figure 5-8 Real-time measurement of efficiency for ET and Class A, third comparison .....	42
Figure 6-1 Regions of operation chosen for comparison of ET and Class A .....	44
Figure 6-2 Region I real-time efficiency data, with illustrations of supply rail voltage and output power	45
Figure 6-3 Real-time efficiency data for Region II comparison.....	46
Figure 6-4 Real-time efficiency data for Region III comparison.....	47
Figure 6-5 Efficiency curves with PDF overlays.....	48
Figure 6-6 Loss of regulation in LLRF system .....	51
Figure 7-1 HBH ET RF amplifier prototype .....	55
Figure 7-2 Efficiency of FRIB prototype power supply for various loads and supply voltage settings .....	56
Figure 7-3 Variable power supply waveforms for 1kHz modulation .....	57



## CHAPTER 1: INTRODUCTION

On March 17<sup>th</sup>, 2014, construction began on the Facility for Rare Isotope Beams (FRIB) in East Lansing, Michigan [1]. The facility has a projected construction budget of \$550 million, and is expected to be completed sometime in the year 2020. The construction progress is monitored daily and can be viewed at [2]. Based on the Michigan State University campus, FRIB will subsume the existing National Superconducting Cyclotron Laboratory (NSCL). NSCL was itself built in 1963, and was also used to conduct research on rare isotopes. Once completed, FRIB will be a valuable tool for continuing this research.

### 1.1 Rare Isotopes

The purpose of FRIB is to study isotopes not often found in nature. Isotopes are variants of elements that contain more or less neutrons than protons in their nucleus. The study of these rare isotopes is important because it can lead to a new understanding of nuclear physics, astrophysics, and the evolution of the universe, while also providing new avenues for technological advancements [3]. The projected isotope production for FRIB experiments are shown Figure 1-1. For interpretation of the references to color in this and all other figures, the reader is referred to the electronic version of this thesis. The black line in the middle of the group shows products that are stable and occur naturally. When an atom has more or less neutrons than it would naturally, it becomes less stable and will more likely decay into smaller parts. FRIB attempts to generate these isotopes by smashing ions into foils of various metals at the end of a linear accelerator. These unstable isotopes can have a very short half-life or very low energy, leading to the necessity to have very sensitive sensory systems.

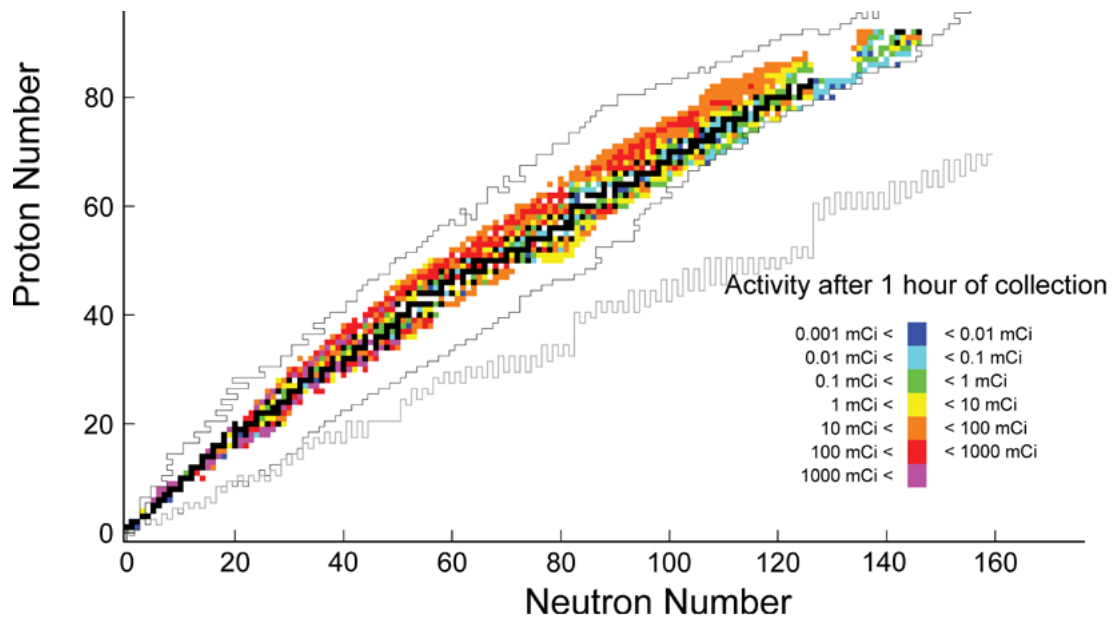


Figure 1-1 Chart of expected FRIB isotope production<sup>1</sup>

Isotopes towards the right side of Figure 1-1 do not occur very frequently and require a large amount of energy for generation in collision, therefore it is beneficial to have a powerful accelerator that can also handle large variety of beams for its experiments. The folded paperclip arrangement shown in Figure 1-2 was chosen to allow for a large scale accelerator while also accommodating for the limited amount of space available on the MSU campus. Particles are ionized and then bunched together in the Front End segment in the center-right portion of the accelerator, then linear accelerator segments and folding segments continue to accelerate the beam and steer it off towards its final destination at the Fragmentation Target. The acceleration process is done largely through the use of cryogenically-cooled superconducting resonant cavities and beam steering is accomplished with large electromagnets. Space is being reserved after the third linear accelerator segment for the inclusion of more resonant cavity systems, which could provide even more acceleration.

<sup>1</sup> ©Copyright by Michigan State University. Reprinted with permission.

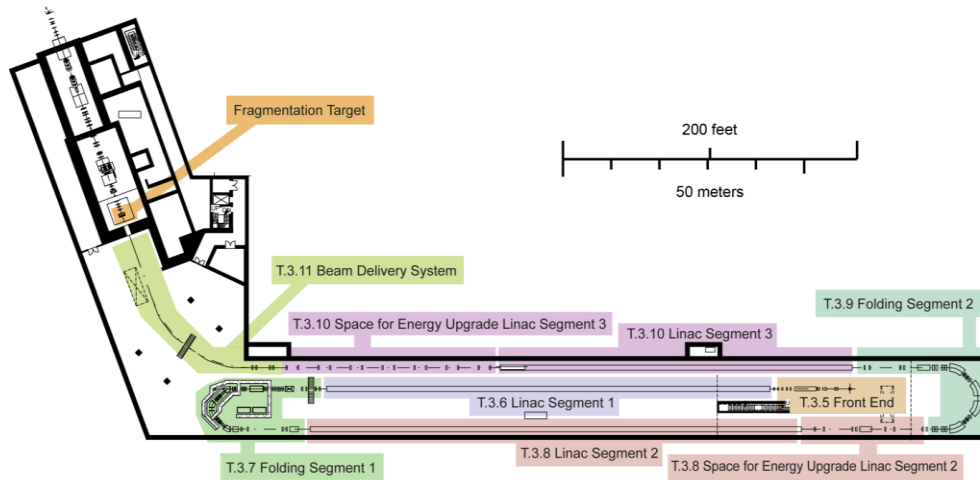


Figure 1-2 Layout of the FRIB accelerator<sup>2</sup>

## 1.2 Superconducting Cavities

As mentioned earlier, one of the main proponents of acceleration on the beamline is the superconducting resonant cavity. A dissection of the various planned cavity types is shown in Figure 1-3. Each of the cavity type designs accelerate the particle beam at different rates; cavities designed for slower rates of acceleration are placed in Linac Segment 1 and are gradually replaced with higher-acceleration cavities farther down the beamline.

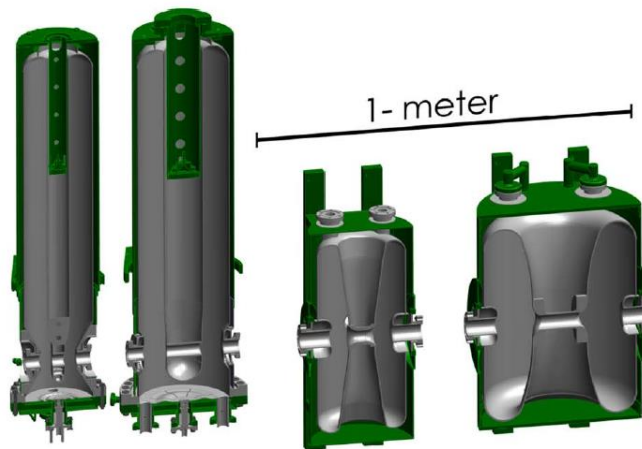
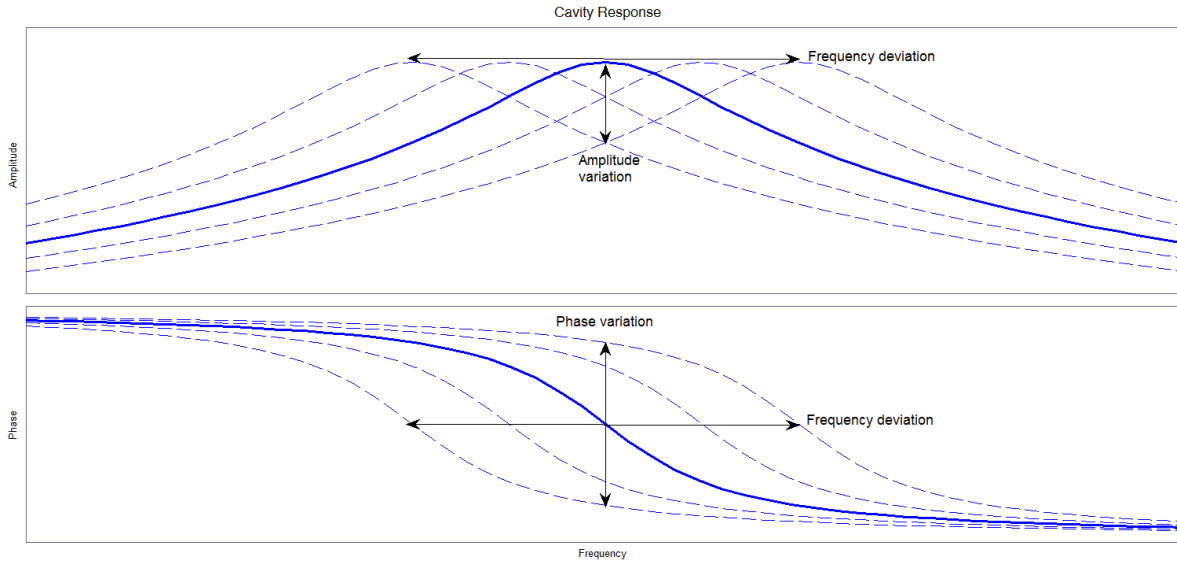


Figure 1-3 Cutaway view of cavities used on beamline<sup>3</sup>

<sup>2</sup> ©Copyright by Michigan State University. Reprinted with permission.

<sup>3</sup> ©Copyright by Michigan State University. Reprinted with permission.

Particle acceleration takes place within the cavities in the following way. Voltage gradients across gaps within the cavity attract and then repels ionized particle bunches as they pass through. This voltage gradient is generated by a radio frequency (RF) signal that is fed into the cavity via a high power amplifier. The frequency and phase of this signal is designed to match the spacing of the ionized particle bunches. The cavities are designed to have an extremely high Q factor, so that the RF voltage amplitude is amplified to the large levels required for the acceleration specification. Having a high Q factor means that a cavity will have little loss of energy, but also a very small operating bandwidth. The cavities are housed within a cryogenic bath to minimize losses from the cavity walls.



*Figure 1-4 Variance of cavity response due to changes in cavity dimension*

Since the resonant frequency depends on cavity dimensions, any variance in a cavity's shape will also affect the frequency it resonates at. The cavity's shape can be altered by several things, including changes in temperature and pressure in the cryogenic bath, and microphonics generated from nearby vibration sources such as vacuum pumps. A depiction of how the cavity's frequency response varies in response to these disturbances is shown in Figure 1-4, where the solid blue line shows the desired amplitude and phase characteristics. Because the cavity is designed with a very high Q, the bandwidth

of this response will be very small and consequently a slight shift will result in a very large drop in amplitude and change in phase.

In an attempt to regulate cavity response, feedback is employed as illustrated in the diagram in Figure 1-5. A probe placed inside the cavity allows monitoring of the amplitude and phase of the voltage gradient. If either the amplitude or phase of the voltage gradient in the cavity varies from the desired set point, multiple forms of compensation are used to correct the error.

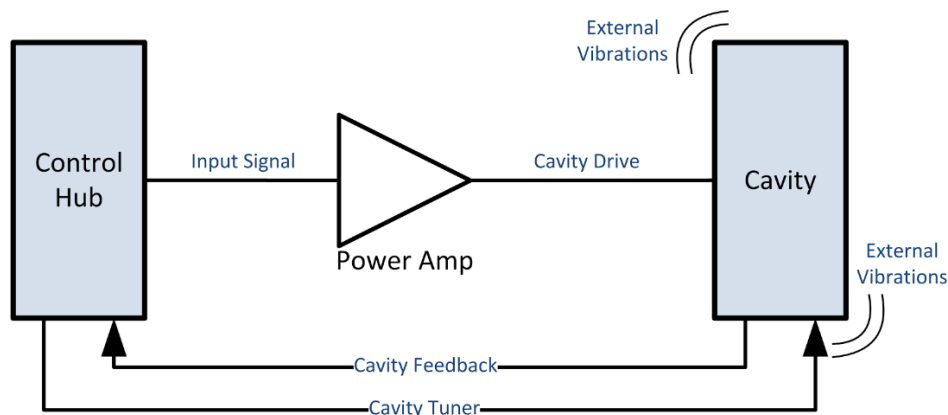


Figure 1-5 Cavity drive block diagram

The first form of compensation is the cavity tuner, whereby a mechanical system is used to change the dimensions of the cavity. This can be carried out in multiple ways, with one such method using a stepper motor to compress or decompress the cavity walls. The tuner is used mainly to compensate for changes in cryogenic bath temperature and pressure that occur over long periods of time. Using stepper motors for tuning purposes will also result in a slight offset from the desired cavity response, since the motors can only deform the cavity walls in finite steps. The tuners are generally not fast enough to deal with microphonics. These issues lead to the need for another compensation system to be included.

The second compensation method employs modulating the RF amplifier signal, where the signal amplitude and/or phase is increased and decreased as necessary to regulate the cavity

response. An example of the RF compensation system at work is shown in Figure 1-6. As microphonics deform the cavity, the feedback network senses this and modulates the RF amplifier's input signal to compensate. This can be seen in Figure 1-6 as the modulation of the top of the power waveform. The power modulation can be analyzed to determine at what frequencies the cavity is vibrating at, allowing for identification of troublesome noise sources. Vibrations at the harmonics of 60Hz, for instance, can most often be attributed to the nearby vacuum pump motors mentioned earlier. This form of compensation is only limited to the bandwidth of the RF system, allowing for correction of higher frequency microphonics.

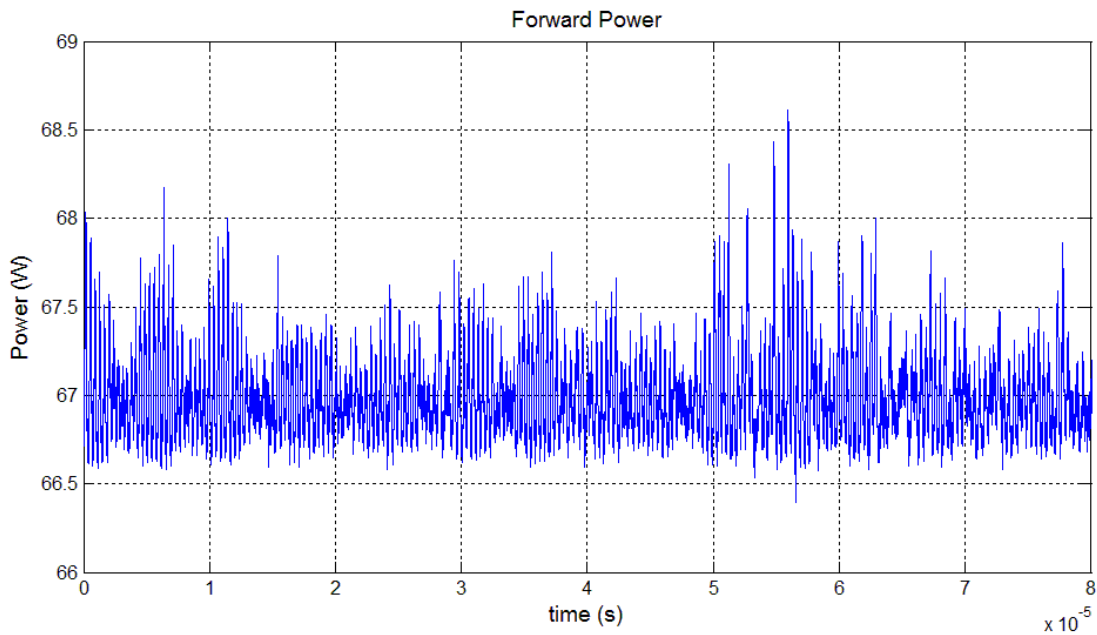


Figure 1-6 Example of RF power modulation used to counteract cavity detuning from microphonics

The mechanical vibrations vary randomly in frequency and amplitude, leading to the amount of output power required by the cavity to also vary randomly. The likelihood of the forward power taking certain values can be characterized with a probability density function (PDF). The PDF generated for the data from Figure 1-6 can be seen in Figure 1-7. The point where the PDF reaches its highest percentage corresponds to the average amount of power the RF amplifier supplied within the given timeframe. This

representation is useful for predicting performance metrics such as average efficiency in systems with randomly varying signals.

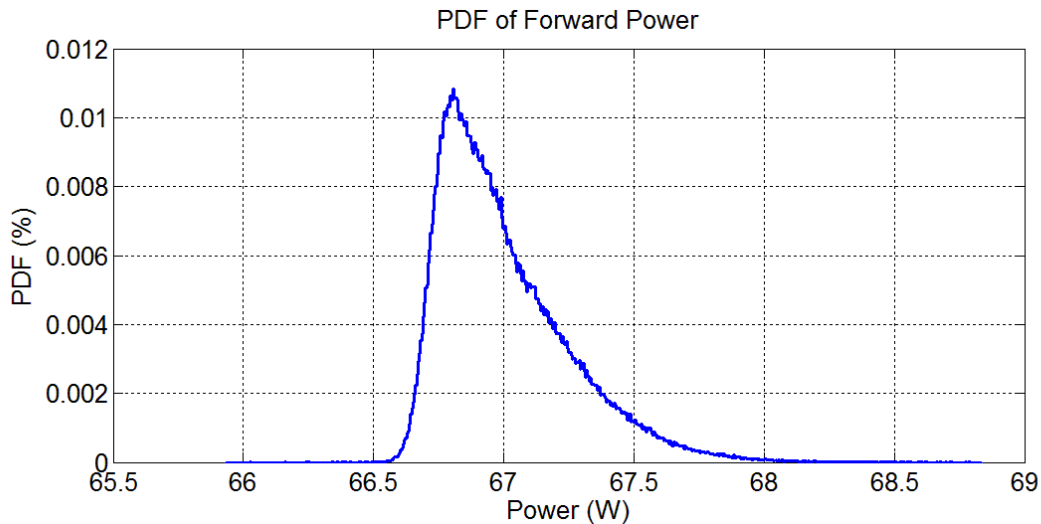


Figure 1-7 Example of probability density function for cavity-drive power

The left-most data point in Figure 1-7 denotes the minimum output power required from the RF amplifier, and corresponds to the points in time when the cavity frequency response was in-tune and centered closest to the target frequency of 80.5MHz. The right-most data point corresponds to the largest amount of power required to counteract cavity detuning from microphonics. The average amount of power actually required from the RF amplifiers will lie somewhere in between these two extremes, with a PDF that will be similar in shape to that seen in Figure 1-7. Design specifications for FRIB require that RF amplifiers be able to handle a dynamic range of at least 3dB, or twice the power required when the cavity is in-tune.

Over the course of its lifetime, the FRIB will be used for a multitude of experiments, each with their own cavity power requirements. Because of this, the RF amplifiers will be designed such that they will be able to handle a wide range of output power requirements. The PDF for each of these experiments should retain the same basic shape and dynamic range, but will be shifted left or right according to the amount of cavity power required.

### 1.3 Envelope Tracking and Energy Savings

In order to facilitate particle acceleration rates of up to half the speed of light, the linear accelerator sections in FRIB use many superconducting cavities. Each of the cavities needs its own RF amplifier to drive it, and the RF amplifiers draw energy from the power grid in order to do so. Because of the large quantity of RF amplifiers present on the beamline, it is important to consider the amount of power they consume and the resulting energy costs.

$\beta$	Qty	Average Power (W)	Efficiency		
			40.0%	50.0%	55.0%
			Power (MW)		
0.041	12	650	0.02	0.02	0.01
0.085	94	2200	0.52	0.41	0.38
0.285	76	2700	0.51	0.41	0.37
0.53	148	4800	1.78	1.42	1.29
<b>Total (MW):</b>			<b>2.83</b>	<b>2.26</b>	<b>2.05</b>

Table 1-1 Projected power usage for RF amplifiers on the beamline

Table 1-1 shows the number of amplifiers required for each type of cavity, the typical average power required to operate these amplifiers, and the total amount of power consumed by the amplifiers. The power consumption columns are further divided into three cases for amplifier efficiency. The first column corresponds to the original estimates with amplifiers that are 40% efficient, while the other two columns illustrate reduction in power consumption if the overall amplifier efficiency could be increased 10% and 15%, respectively. Table 1-2 shows the corresponding energy cost estimates for each amplifier efficiency case. For a 10% increase in efficiency it is possible to save more than \$200k annually, and for a 15% improvement it is possible to save more than a quarter of a million dollars a year in energy costs. These potential savings motivated the search for higher-efficiency amplifier options.



		Efficiency		
		40.0%	50.0%	55.0%
cost/MW hr	hour/year	Cost per year		
\$70	5500	\$7508	\$6006	\$5460
		\$199045	\$159236	\$144760
		\$197505	\$158004	\$143640
		\$683760	\$547008	\$497280
	<b>Total (\$M):</b>	<b>\$1.09</b>	<b>\$0.87</b>	<b>\$0.79</b>
	<b>Delta to 40%:</b>	<b>\$0.000</b>	<b>-\$0.220</b>	<b>-\$0.300</b>

Table 1-2 Projected energy cost savings for increased efficiency

One method to improve efficiency of RF systems is that of envelope tracking (ET). The ET method involves modulating the RF power amplifier’s supply rail voltage in accordance with the envelope of its output voltage, keeping the difference between the two nearly constant. Since an amplifier’s efficiency is related to this difference, it too will be constant [4] [5]. ET also allows amplifiers to maintain a high degree of linearity, whereas classic amplifier topologies usually have an inherent tradeoff between linearity and efficiency [6]. These details provided the motivation to inspect ET as a valid candidate for achieving the aforementioned efficiency numbers for the FRIB amplifiers.

#### 1.4 Thesis Layout

This thesis investigates the implementation of an ET architecture as it would be used in the FRIB cavity-drive scenario and examines the possible efficiency gains to be had from using such an arrangement. Chapter 2 will discuss ET in greater detail and compare it to traditional RF amplifier topologies. Chapter 3 will detail the initial steps of the ET system design with characterization of the test amplifier. The design process for the ET control algorithm will be given in Chapter 4 along with an explanation of the test setup to be used in the ET experiments. Chapter 5 will explore the results of initial ET tests without microphonics while also verifying functionality of the ET algorithm. Chapter 6 will introduce microphonics into the ET test setup and discuss the results of doing so. The final chapter will offer some insight into the practical considerations for ET and expound on future work to be done at FRIB.

## CHAPTER 2: ENVELOPE TRACKING AMPLIFIERS

A detailed discussion on ET will be given in this chapter. Preceding this will be a description of classic RF power amplifier designs so that the gains of envelope tracking can be easily exemplified. A detailed explanation of how ET can improve performance will then be given, along with some discussion of research that has been done with ET technology. The details given in this chapter will be crucial to the understanding of the ET test results that will be shown in later chapters.

### 2.1 Classic RF Power Amplifier Design

Before examining ET, it is important to know the issues with traditional RF power amplifier design. It is typical for traditional RF power amplifiers to operate with a single-ended or push-pull design, employing a Class A, B, AB, or C mode of operation. Because these amplifier topologies use a constant supply rail voltage, there is an inherent tradeoff between efficiency and linearity, as will be shown.

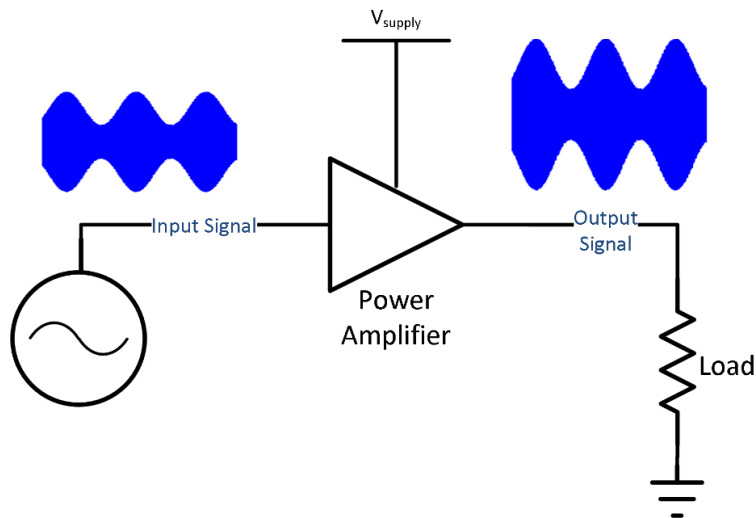


Figure 2-1 Block diagram for static-supply amplifier

A simple power amplifier configuration with an amplitude-modulated (AM) signal is shown in Figure 2-1. The input signal would typically originate from some low-power, highly linear preamplifier

stage. The power amplifier takes energy from the power supply and uses it to amplify the input signal, creating usable power that is transmitted to the load. Because this conversion is not perfect, some power will be dissipated in the power amplifier itself in the form of heat. The efficiency for the power amplifier is the ratio of the power sent to the load and the power supplied to the power amplifier such that:

$$\eta [\%] = 100\% \times \frac{P_{out}[W]}{P_{supplied}[W]} \tag{2-1}$$

It should be noted that this definition of efficiency is for the power amplifier alone and does not include any losses in the power supply itself. The total efficiency for a system is the product of the efficiencies of its independent parts, so that a system with a 60% efficient power amplifier and an 80% efficient power supply would result in a total efficiency of 48%. It is generally safe to assume that most of the current drawn by the power amplifier goes through the drain(s) of the amplifier’s output transistor(s), and so the efficiency of the power amplifier is usually termed “drain efficiency” for further clarity.

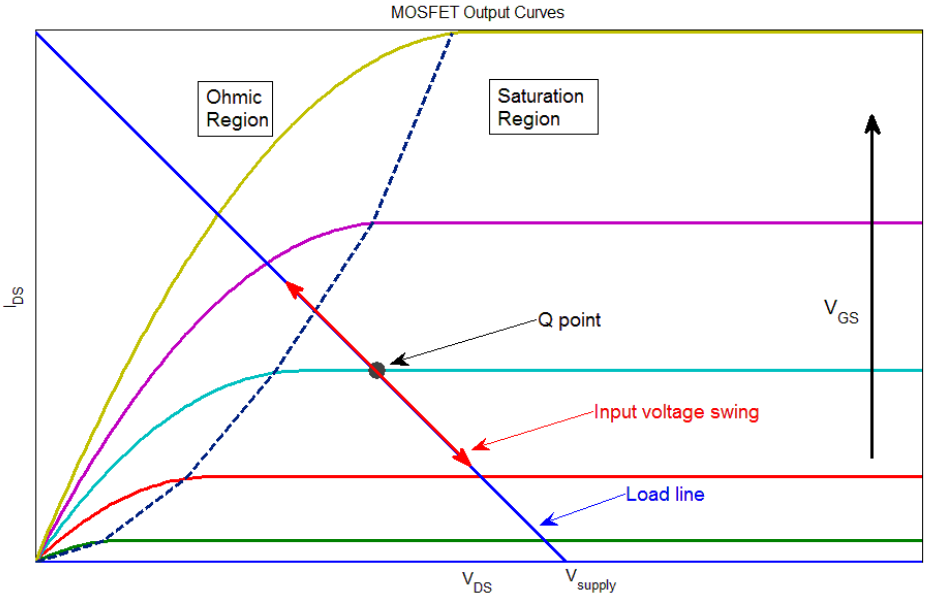


Figure 2-2 MOSFET output characteristics

For AM waves, information is carried in the modulation of a high frequency carrier wave. Proper transmission of information from the signal source to the load would require the power amplifier gain to be constant. This is referred to as linear operation, so called because the output signal is just a linearly-scaled version of the input signal. Unfortunately, the gain of an amplifier is not constant for all possible input amplitudes. For power amplifiers that are based on a single transistor device, the reason for this can be seen by looking at a transistor's output characteristics. An example MOSFET characteristic diagram with load line is shown in Figure 2-2. The drain of the MOSFET is biased at the quiescent point by the load resistance as shown in the diagram. The drain-source voltage and drain-source current will vary on these curves according to the swing of the gate-source voltage. When the drain-source voltage is in the saturation region on the right side of the plot, the transconductance of the MOSFET will be constant, corresponding to a constant power gain. When the gate-source voltage is at the peak of its positive swing, the drain-source voltage is in the nonlinear Ohmic region and the MOSFET's drain current no longer varies linearly. This results in lower gain and the output signal will no longer be a linearly-scaled copy of the input signal.

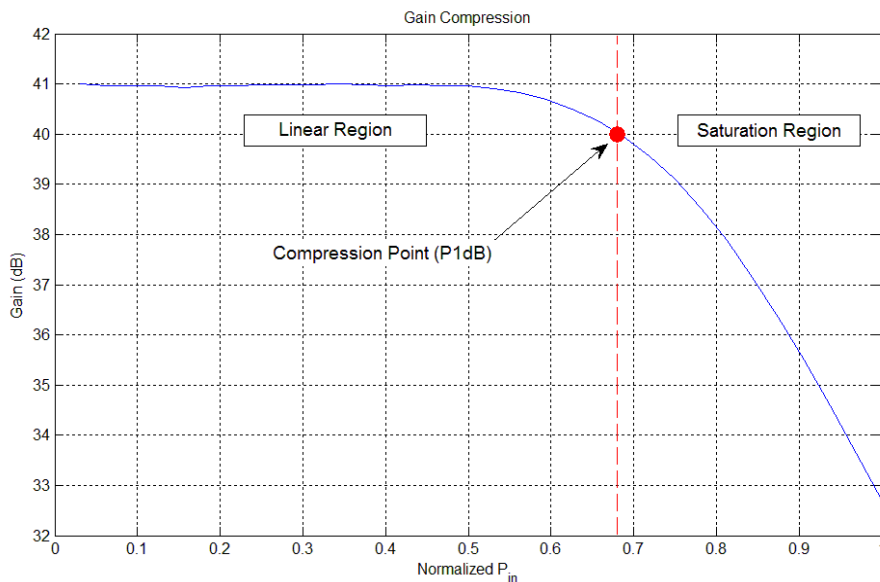


Figure 2-3 Gain compression for a RF amplifier

A common way of representing gain variance with RF amplifiers is shown in Figure 2-3, where gain is compared against input power. It can be seen that for low values of input power, the amplifier gain is a constant value. As the input signal amplitude increases past the MOSFET's saturation-Ohmic threshold, however, the amplifier gain steadily decreases. This effect is called “gain compression” or “saturation” in the power amplifier [6]. The point at which the gain has decreased by 1dB from its linear region value is called the P1dB; a commonly used metric for RF amplifier performance.

When the amplifier is saturated, its output signal will no longer be a linearly-scaled copy of the input signal, and the difference between power coming out of the amplifier and power going into it will decrease. It is common practice to operate the amplifiers in a “power back-off” mode, where the rated operating range of the amplifier is such that the maximum allowable input power does not exceed the P1dB point [7] [8] [9]. This technique guarantees linearity of the amplifier at the cost of efficiency, the reasons for which will be in the following discussion.

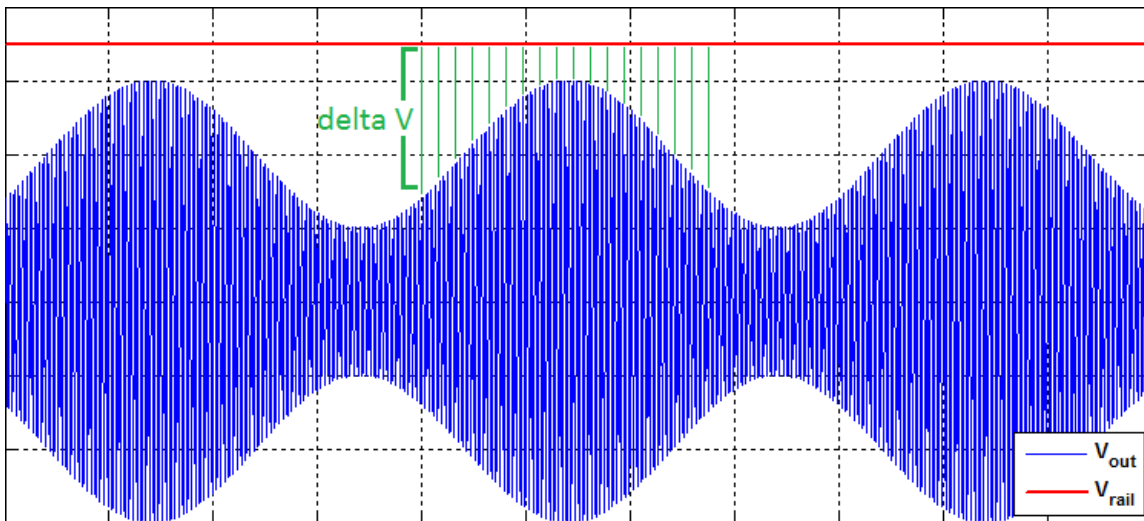


Figure 2-4 Comparison of drain voltage to rail voltage for classical amplifiers

Amplifier operation can also be analyzed in terms of drain voltage and time. Figure 2-4 shows an example AM voltage waveform taken from the drain of an amplifier's transistor and compares it to the constant supply rail voltage. As the value of the drain voltage amplitude approaches that of the

supply rail voltage, the amplifier gain will decrease and the top of the drain voltage waveform will become clipped. This clipped voltage waveform corresponds to nonlinear operation, which results in the generation of undesired harmonics. Since power is directly related to voltage, the ratio of output power to supplied power can be related to the ratio of drain voltage to supply voltage. The instantaneous efficiency of the amplifier will vary in time then with the difference between the supply rail voltage and the drain voltage. The green “delta V” lines in Figure 2-4 highlight this relationship. Longer delta V lines correspond to lower efficiency, and vice versa. Figure 2-5 exemplifies this principle further by looking at how efficiency and gain vary simultaneously with output power. As output power increases, efficiency increases but gain decreases. If the difference between the supply rail voltage and drain voltage can be controlled, this relationship can be rectified to linearize gain and improve efficiency.

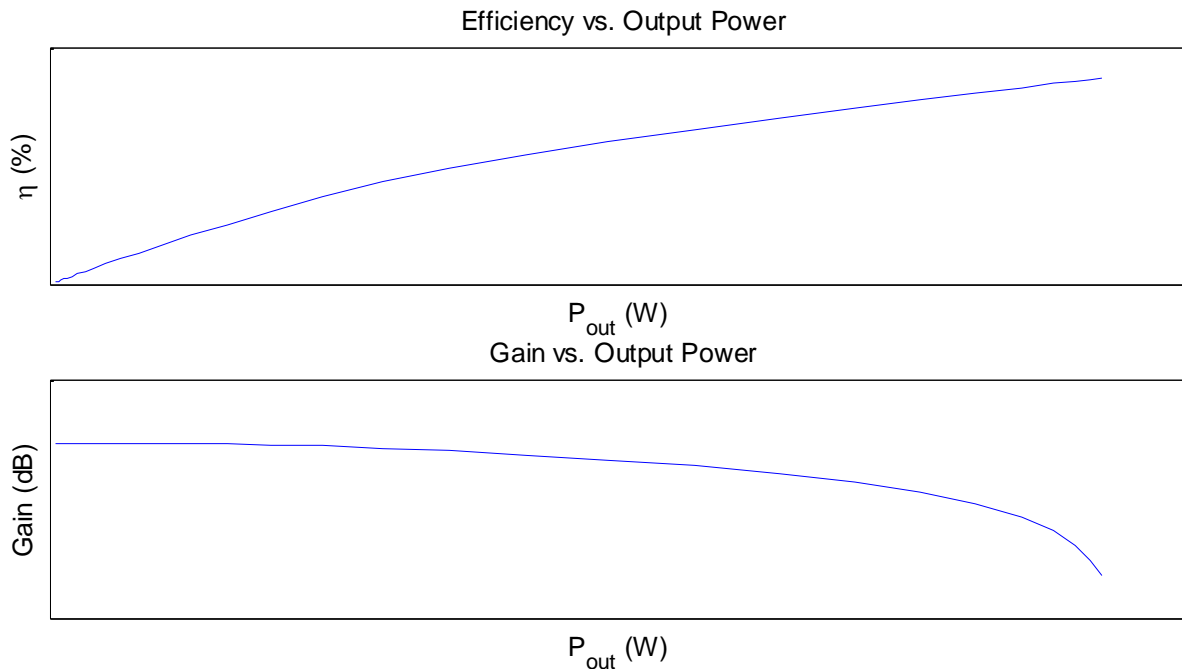


Figure 2-5 Variance of efficiency and gain with respect to output power for a constant rail voltage

## 2.2 Envelope Tracking

A block diagram for an ET amplifier is shown in Figure 2-6. The input AM signal is first fed through or generated by a control system that detects the envelope shape and then uses it to generate the supply modulation waveform. In order to ensure alignment between supply and output signal envelope, a certain amount of time delay is implemented in the control system as well. The supply modulation waveform is sent to an envelope amplifier, which scales it up to the voltage necessary to power the power amplifier. The power amplifier itself is usually comprised of a one- or two-transistor design and is biased as a Class A, B, C, or AB device.

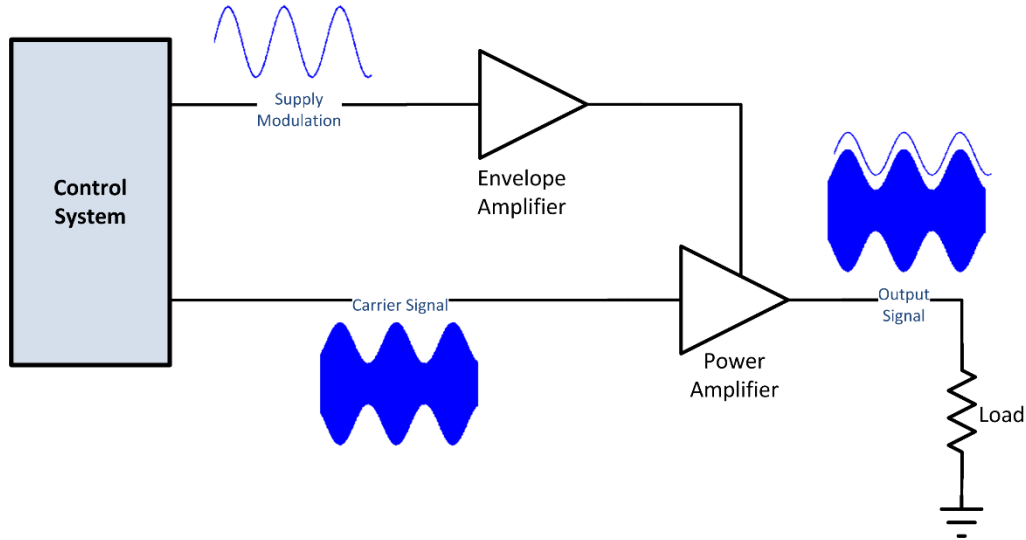


Figure 2-6 Block diagram for ET amplifier

The linearity and efficiency characteristics of a RF power amplifier both depend on supply rail voltage. Figure 2-7 shows how efficiency and gain change for a power amplifier with various supply rail voltages, with the lowest rail voltage curve on the far left and the highest rail voltage curve on the far right. The black dashed line in the figure shows the resulting efficiency and gain characteristics are changed when an ET system is implemented for that same power amplifier. For lower rail voltages, the power amplifier has higher overall efficiency than any of the other cases but is limited in the amount of

power it can output. This can be seen in the steep drop in the leftmost gain curve. As the rail voltage is increased, the overall efficiency for the amplifier is lower but it has flat gain for a wider range of power.

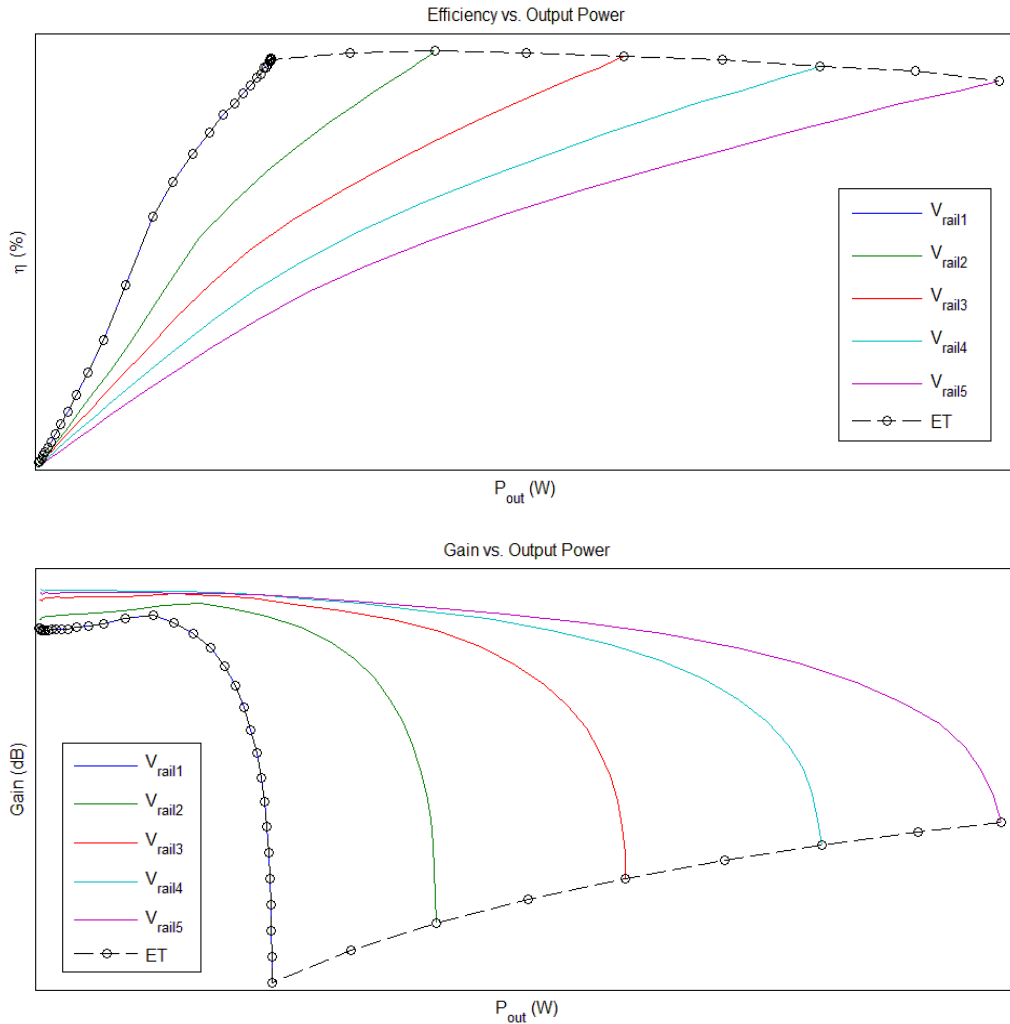


Figure 2-7 Efficiency and gain characteristics for an amplifier with various rail voltages and with ET

There are three regions of operation at work in ET. The first of these is the linear region, where the output power is very small. When the output power is small, the supply rail voltage does not follow the envelope but is instead held at some constant value so as to avoid gain collapse in the amplifier [10] [11] [12] [13]. Here the amplifier operation is identical to that of the traditional constant rail voltage classes mentioned previously, with efficiency that varies with output power and high linearity. This is the reason why the ET curve overlaps the leftmost efficiency and gain curves in Figure 2-7.



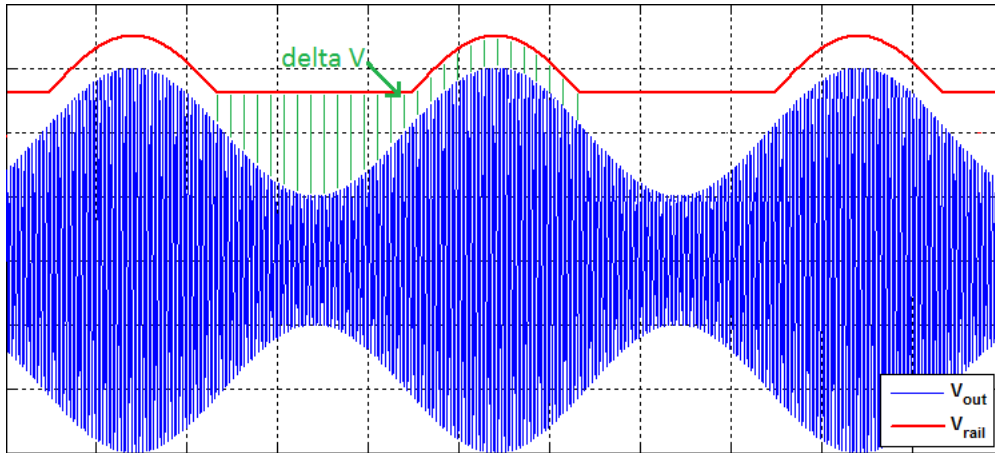


Figure 2-8 Comparison of drain voltage to rail voltage for ET amplifier at modulation threshold

As output power increases and the signal voltage approaches the constant rail voltage, the ET system begins to modulate the supply rail voltage. The voltage waveforms for this region are shown in Figure 2-8. During this time the instantaneous efficiency can be seen to vary during the low part of the swing and then remain constant as the signal peaks. As the supply modulation comes on, the amplifier is actually in saturation and its drain voltage depends on the rail voltage rather than the input voltage [14]. This can be seen in the gain characteristics in Figure 2-7, where the leftmost gain curve has dropped off far from the P1dB point. The gain of the ET scheme can be corrected by modulating the supply voltage in such a way that the transition between linear and saturated regions is smooth and the gain line is made flat again [14]. This will result in a loss in overall efficiency in the ET system, but the trade-off may be worth it depending on the application.

As the amplifier is driven harder, ET will modulate the supply voltage during the entire signal swing. An example of this is shown in Figure 2-9. The amplifier will become fully saturated at this point, and so its drain voltage will be controlled only by the supply waveform. This mode of operation accounts for the nearly flat efficiency portion of the plot in Figure 2-7. With the amplifier in full saturation, the efficiency is almost constant throughout the signal swing. Because of this behavior, it is

possible to have a power amplifier that has high efficiency, high power, and, if optimized for it, high linearity.

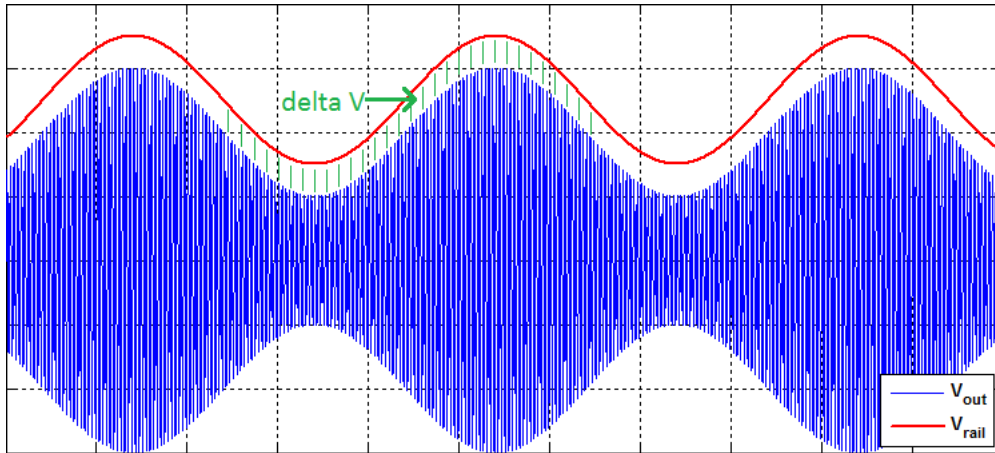


Figure 2-9 Comparison of drain voltage to rail voltage for ET amplifier in full saturation

Many RF applications require amplification of signals with very wide bandwidths and high peak-to-average power ratios (PAPR). Ideally, the envelope amplifier would follow the modulation of these signals perfectly to maximize efficiency. In reality there is often a tradeoff between bandwidth and efficiency with the available choices in envelope amplifier technology. It is important that the envelope amplifier be as efficient as possible as the total efficiency for an ET amplifier is mainly dependent on the product of efficiencies for the envelope and power amplifiers [10]. The envelope amplifier should also be linear enough so that any error introduced by modulating the supply voltage can be accounted for in other parts of the ET system [15]. Using a linear regulator for the envelope amplifier would allow for wider-bandwidth supply voltages at the cost of lower efficiency. If instead a switched-mode power supply (SMPS) is used, the envelope amplifier will have high efficiency but only for a limited bandwidth. Possible switching noise from a SMPS would also have to be factored into the ET design.

Much research has been done in an attempt to get the best of both worlds. A common technique is to use an envelope amplifier that runs both a linear regulator and SMPS in parallel [10] [11] [12]. Another technique involves having multiple regulators, each with different operating bandwidths,

and using control systems to select whichever regulator is appropriate for a given signal amplitude [16] [17] [18]. Still other techniques employ using only a SMPS for the regulator, and using bandwidth-reduction algorithms to modulate the supply at a much slower rate than the signal modulation [15] [19].

The generation of the supply modulation waveform has also been the subject of much research. Many ET techniques focus on creating a bandwidth-limited version the input signal modulation via low pass filtering. After filtering, algorithms are usually employed to remove crests and troughs in the waveform [11] [20] [21] or to create a moving average [18] [19] [22]. Other techniques have used look-up tables (LUT) that take a known set of amplifier characteristics and use them to predict the best supply rail voltage for a given input signal voltage [14] [23].

In order to correct for inaccuracies generated by modulating the supply voltage, digital predistortion (DPD) of the RF input signal is also employed. DPD counteracts nonlinearity in the power amplifier by using feedback to detect harmonics in the output signal and reduce their amplitudes by changing the harmonic content of the input signal. The use of this technique with various algorithms can be seen in [11] [14] [15] [21] [22] and [23].

The next chapter will focus on the characterization of the power amplifier that would be used for the ET experiments. The characterization of the amplifier would allow for the creation of numerous data tables, which would then be used to generate an ET control algorithm in later chapters. The results of the characterization tests should show some agreement with the amplifier operation principles discussed here.

## CHAPTER 3: CHARACTERIZING THE POWER AMPLIFIER

In order to create the ET control algorithm for supply rail voltage modulation, a set of data tables had to first be developed. In order to create these tables, the power amplifier had to be characterized. This chapter will take a look at how the characterization process was carried out using the equipment available at FRIB. A discussion of the results of this test will also be given, with verification of the principles introduced in the previous chapter.

### 3.1 Characterization Test Setup

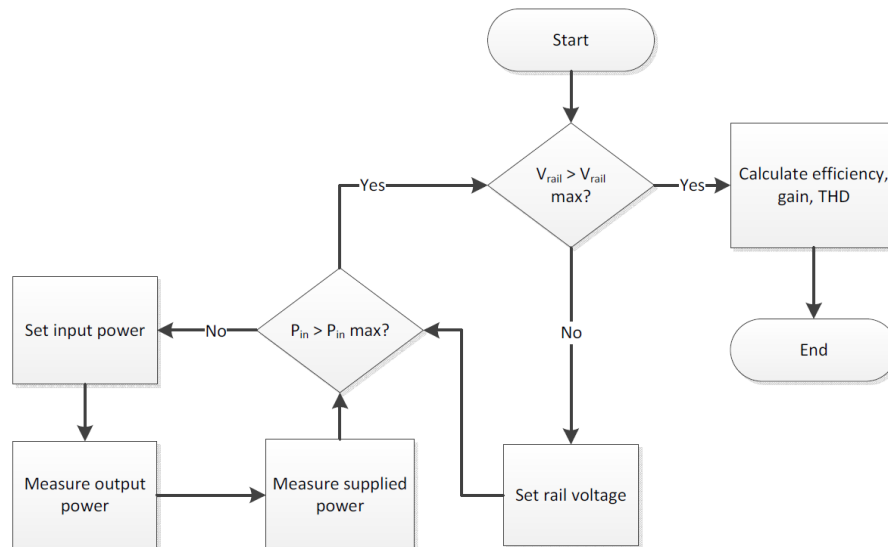


Figure 3-1 Block diagram for characterization tests

The characterization tests measured how the power amplifier's gain, total harmonic distortion (THD), and efficiency changed with respect to input power and supply rail voltage. A flowchart for the proposed test scheme is shown in Figure 3-1, and a block diagram for the equipment setup is shown in Figure 3-2. The test started with setting a rail voltage, then output input power was swept over a desired range. Output power, harmonic power, and supplied power were measured for the power amplifier and used to calculate gain, THD, and efficiency for the amplifier. The entire test was automated using MATLAB software, with the scripts used for the tests provided in Appendix A.2.

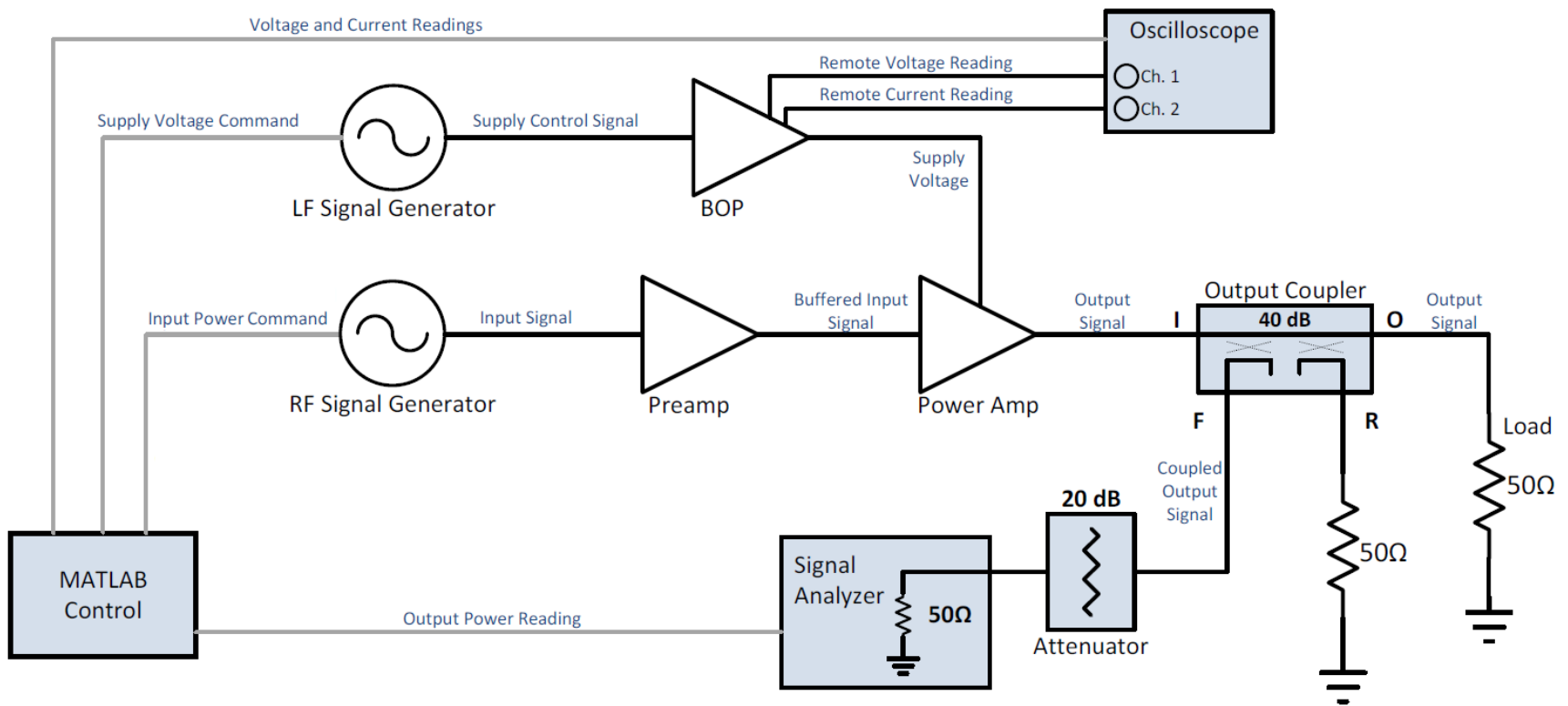
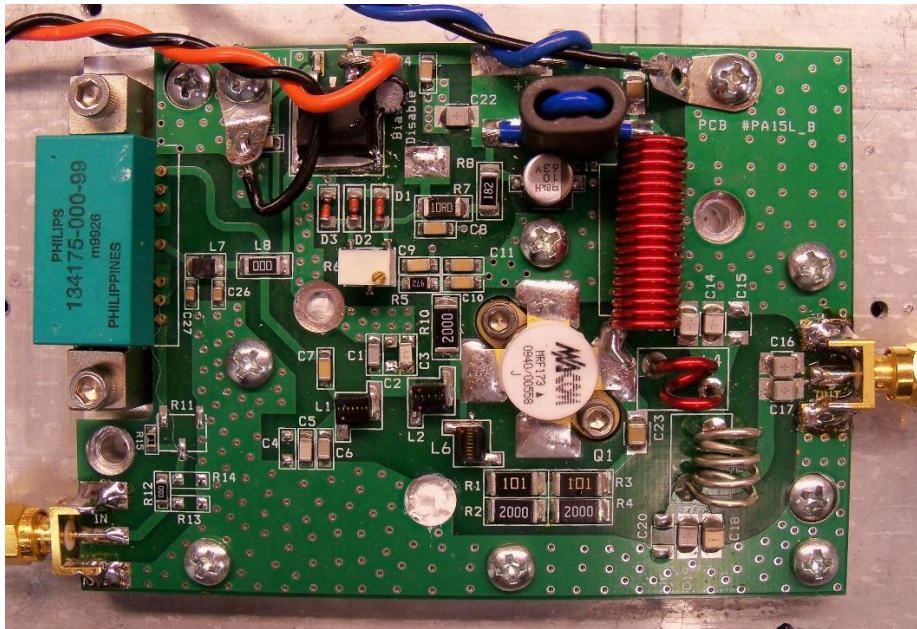


Figure 3-2 Experiment setup for characterization tests



*Figure 3-3 Broadcast Concepts 55-88MHz 12W VHF TV model pallet amplifier*

The power amplifier that was used in these tests is shown in Figure 3-3. The amplifier is based around a single power MOSFET and was originally designed to be operated as a Class A device. The amplifier was also designed by the manufacturer to operate in power back-off to maintain linearity. This was achieved by choosing a power MOSFET whose normal operating region was rated much higher than the intended range of use.

A bipolar operational amplifier power supply (BOP) was used as the power supply and later envelope amplifier. The BOP was a linear device and as such had wide bandwidth, low noise, low distortion, and low efficiency when compared to a SMPS of similar ratings. The BOP used had built-in current and voltage monitors that output their readings on a 0-10V scale, so that an oscilloscope could easily measure the BOP's output. Measurements taken from the scope were rescaled to their actual values using MATLAB.

The FRIB energy consumption estimations that were shown in Chapter 1 only looked at relative efficiency gain, and as such it was decided to only analyze ET improvements in drain efficiency rather than overall efficiency. The efficiency of the BOP itself was not factored into the experiments presented in this thesis, but experiments that are interested in total system performance should factor in the efficiency of envelope and power amplifiers.

The input power signal was chosen to be varied from -15dBm up to 16dBm in +1dB steps. In order to make sure that the signals input to the power amplifier reached these levels, a preamplifier was used to buffer the signal coming from the RF signal generator. The model of preamplifier used was chosen so that it would be linear over the whole range of expected input power values. This would guarantee that any measured variance in gain was due solely to power amplifier behavior.

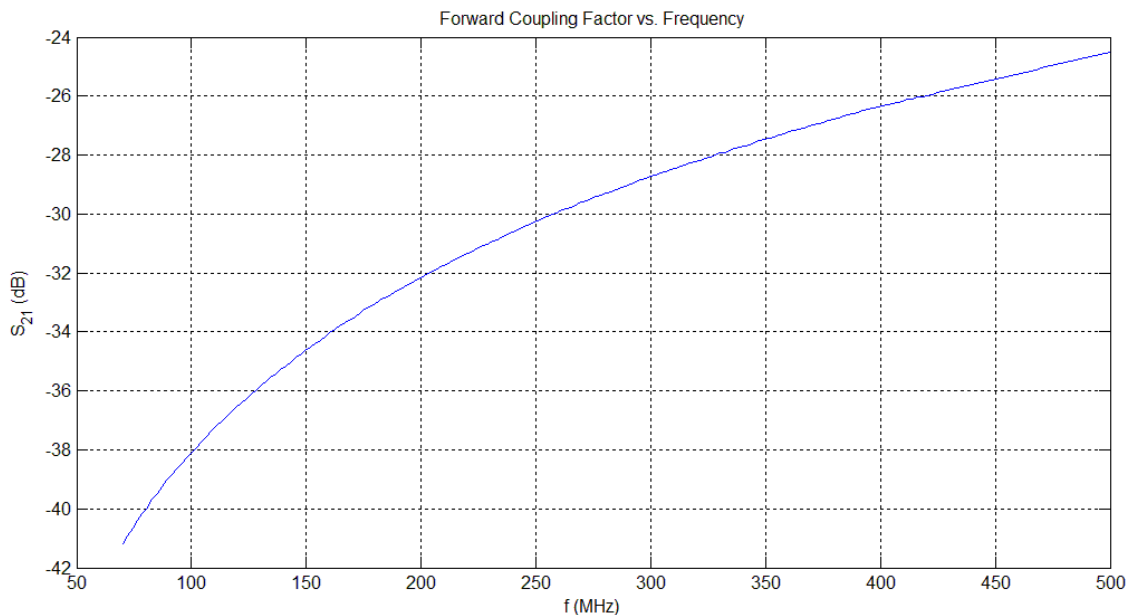


Figure 3-4 Directional coupler forward coupling factor vs. frequency

A directional coupler was used to allow measurement of output power with a signal analyzer. The coupler used was originally designed for 40dB of coupling at a target frequency of 80.5MHz. The directional coupler was designed for a single frequency, and as such its coupling factor had to be

characterized with a network analyzer to allow for accurate measurement of the harmonics of 80.5MHz. The results of such a test are shown in Figure 3-4, where it can be seen that coupling factor increases with frequency. A calibration set based on the results in Figure 3-4 had to be employed in MATLAB to measure output power and harmonic power as they appeared at the output of the power amplifier. The signal analyzer was setup to measure up to the sixth harmonic of 80.5MHz.

For the characterization tests presented here, it was decided that the power amplifier would be tested with a supply rail that varied from 12V to 30V in 2V steps. The 12V lower limit was chosen after determining that rail voltages lower than 10V resulted in gain collapse in the power amplifier. The 30V upper limit was chosen after observing that supply voltages above 36V caused the amplifier to oscillate.

### 3.2 Characterization Test Results

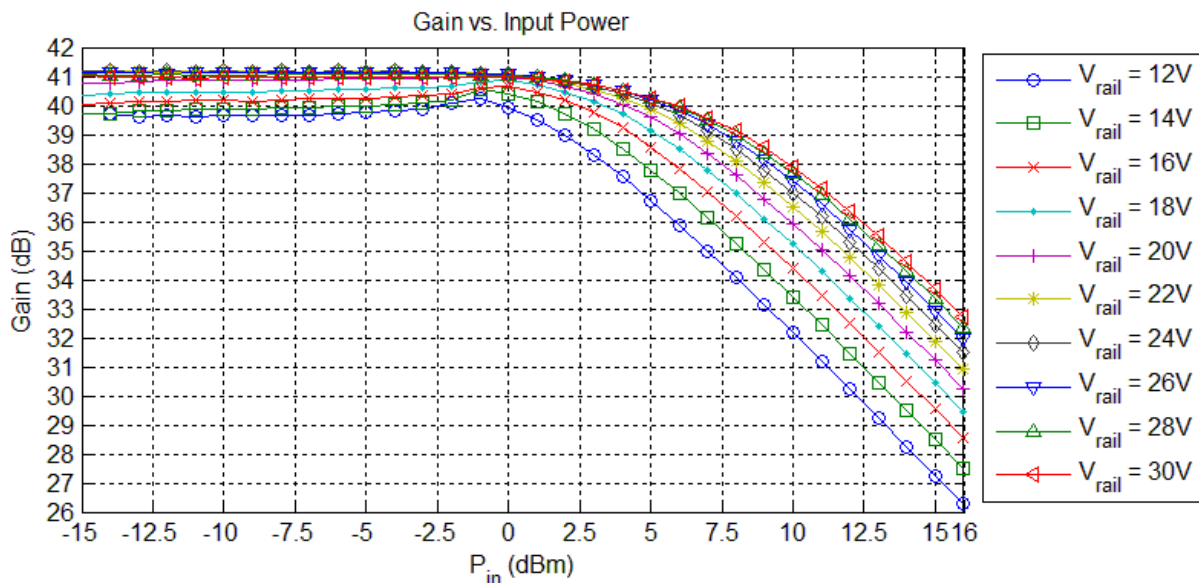


Figure 3-5 Measured pallet amplifier gain vs. input power for various supply voltages

The results of the characterization tests were first used to compare the power amplifier’s gain against input power. The results for this comparison are shown in Figure 3-5. For input power less than 0dBm, the amplifier is acting as a linear device with constant gain. As the input power continues to rise, the amplifier saturates and the gain begins to decrease. The data shows that the lower the rail voltage



is, the less input power it will take to reach the compression point for the amplifier. With higher rail voltages, the compression point moves farther to the right on the graph.

The maximum input power rating for the amplifier was listed by the manufacturer as 0dBm, with a rated rail voltage of 24V or more [24]. Tracing these points on Figure 3-5 reveals that the amplifier does still have constant gain at this power level, and does not reach gain compression until the input power is increased to 5dBm. The fact that the manufacturer’s input power rating is set to be lower than the compression point of the power amplifier is a practical example of operating in power back-off, as discussed in Chapter 2. It is also worth noting that for rail voltages of 24V and above, the separate gain curves follow each other closely. This could have been part of the manufacturer’s justification for rating the amplifier for rail voltages above 24V, since the power amplifier’s gain would be more consistent between a 24V and 30V rail than between a 12V and an 18V rail.

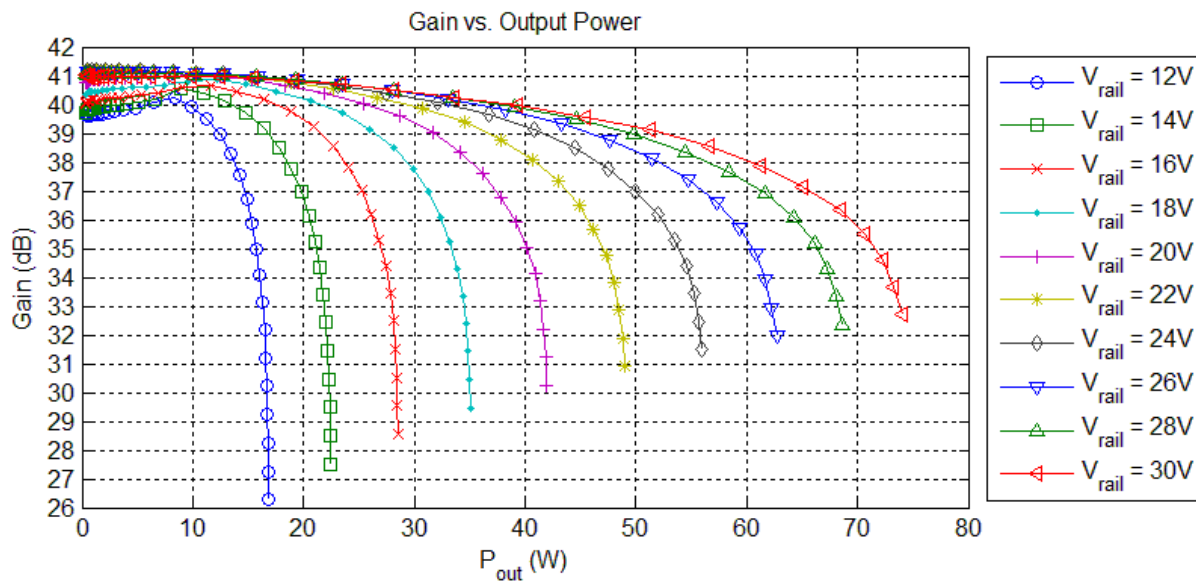


Figure 3-6 Measured pallet amplifier gain vs. output power for various supply voltages

Gain was also analyzed with respect to output power, as shown in Figure 3-6. A similar trend can be seen here as in the previous gain measurements, where the amount of gain available drops as the amplifier becomes saturated. Here it is also possible to see that when the amplifier saturated, its

output power approached a limit. As the amplifier saturates, more power will go into harmonics of the output signal while the rate of increase in fundamental power will decrease.

When the amplifier is operating in the linear region, the output signal will be a linearly-scaled version of the input signal. As the amplifier enters saturation it becomes a nonlinear device, and the output signal will no longer be merely a scalar multiple of the input signal. This nonlinear behavior causes higher frequency harmonics of the fundamental signal to be generated. THD is the ratio of the sums of the power in the harmonics to the power in the fundamental.

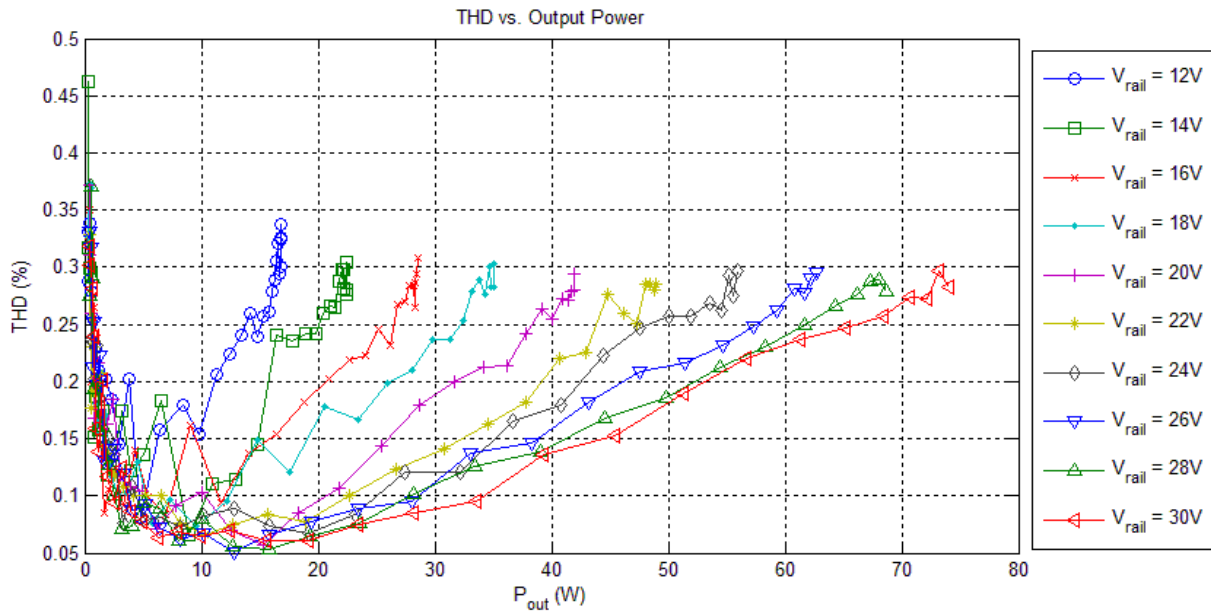


Figure 3-7 Measured pallet amplifier THD vs. Output Power

The analysis of THD was performed with respect to output power, as shown in Figure 3-7. The increase in THD at lower output power levels was an artifact of the way the signal analyzer measured signals; the span of the signal analyzer was setup so that the fundamental and its first five harmonics were able to be shown on the screen. Having a wide measurement span also resulted in a higher noise floor. For lower output power levels, the fundamental and its harmonics were of similar magnitude to the noise floor. This resulted in a rise in THD as the harmonics appeared to be of similar magnitude to

the fundamental. Accuracy for lower-power signals can be increased by decreasing resolution bandwidth for the signal analyzer measurements, at the expense of measurement speed.

When the supply rail was set to a lower voltage, THD rose more quickly with increasing output power. Just as was the case for the gain measurements, the amplifier's linear operating range was expanded with higher rail voltages. The amplifier had lower distortion when it was operating linearly and its gain was constant. As the amplifier entered saturation, the gain began to decrease and distortion also increased.

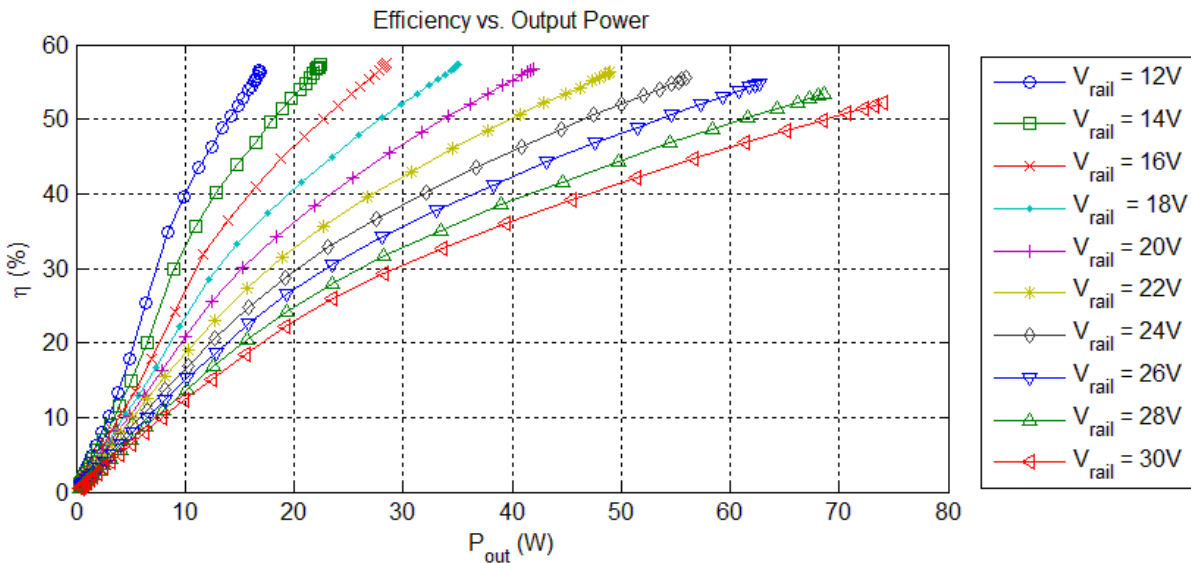


Figure 3-8 Measured pallet efficiency vs. output power

The last of the analysis looked at efficiency measurements. A comparison of efficiency with respect to output power and supply rail voltage is shown in Figure 3-8. When the rail voltage was lower, it was possible to get higher efficiency at lower output power levels. A lower rail voltage also limited the maximum amount of output power that could be drawn from the amplifier, so that higher output power requirements necessitated higher supply rail voltages. With the efficiency data compared against output power, it is possible to find the lowest rail voltage necessary to maximize efficiency while still delivering some desired amount of power. If, for example, the amplifier were expected to deliver 40W

of power, the graph can be consulted to show that a supply voltage around 20V would provide the highest efficiency at around 55%. This method of maximizing efficiency was used to develop an ET control algorithm later.

After completing the characterization tests, all of the data was compiled into accessible reference tables. The next chapter will take these tables and use them to create the ET control algorithm. The data will have to be manipulated in such a way as to work with the control equipment that was readily available at FRIB, meaning that some compromises would have to be made.

## CHAPTER 4: CONTROL ALGORITHM DEVELOPMENT

This chapter will focus on how the control algorithm for the ET supply waveform was developed. The control algorithm had to be tailored to the hardware it would be used with, and as such a discussion of how the FRIB cavity drive problem was emulated on the test bench is necessary. Since the simulation was created using equipment that was readily available at FRIB, some compromises had to be made between performance and measurement accuracy.

### 4.1 Test Bench Setup

A block diagram of the full ET test bench setup is presented in Figure 4-1. The gray lines in the figure represent communication connections between the PC and hardware, and the black lines represent RF signal paths. The ET setup was similar to the power amplifier characterization setup used in the previous chapter, but with the addition of a feedback loop for supply voltage control. A low-level RF control system (LLRF) was used as the control hub for the ET experiments. The LLRF was designed by engineers working at FRIB to regulate the amplitude and phase of superconducting cavity signals to correct for disturbances due to microphonics and variations in cavity dimensions [25] [26].

It was the duty of the LLRF to generate the supply modulation and RF drive signal waveforms, as well as take in feedback signals for error correction in the ET setup. Control with the LLRF worked by measuring the amplitude and phase of the RF feedback signal and comparing them against a programmed set point. If the feedback voltage was greater than or less than the desired set point voltage, the LLRF would decrease or increase the outgoing RF signal drive, respectively. The LLRF can be calibrated to offset attenuation levels present in the feedback loop, permitting the monitoring of output power levels as they appear at the power amplifier output.

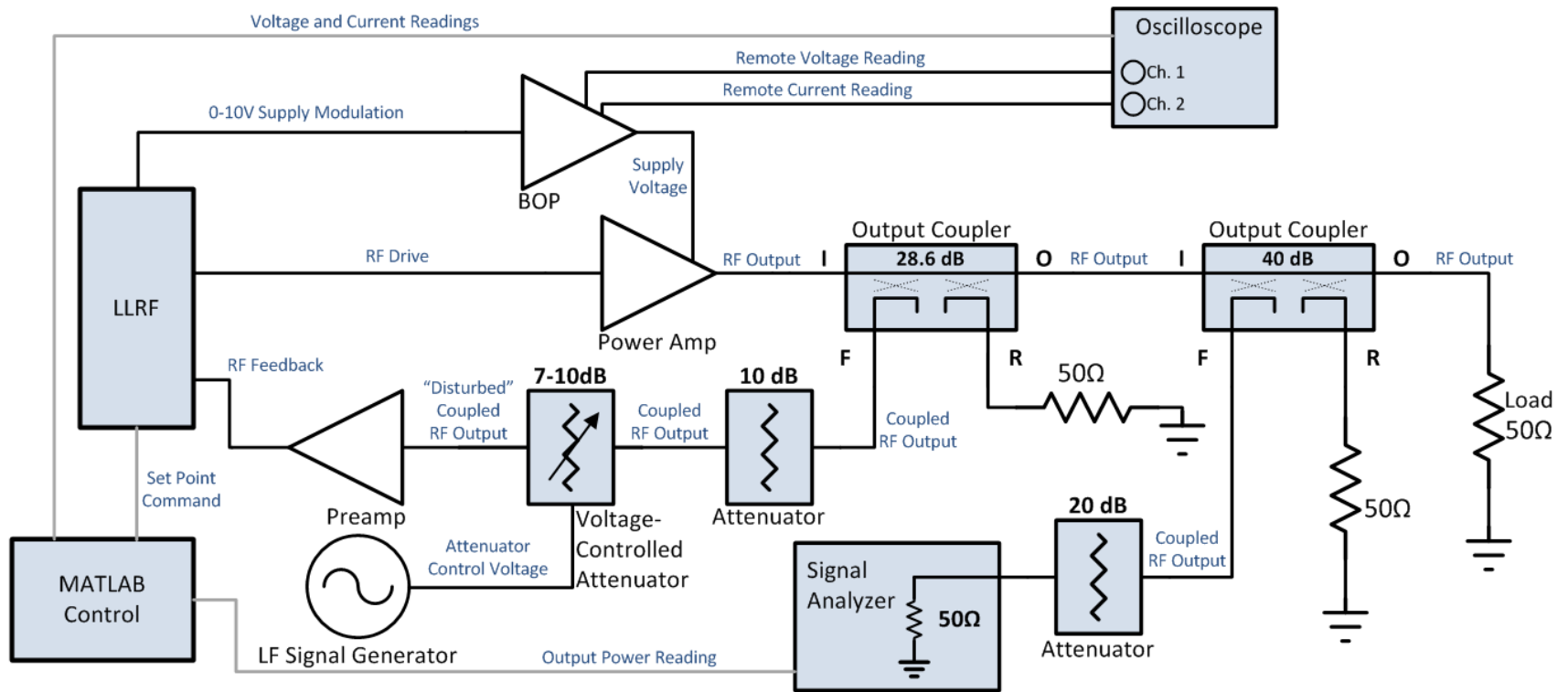


Figure 4-1 ET experiment setup block diagram

In order to simulate a cavity control environment on the test bench, a feedback path had to be provided that would allow the LLRF to monitor the RF output signal. The feedback path was created using equipment readily available at FRIB. A second directional coupler was added in-line with the RF output signal path to facilitate a feedback breakoff point while still allowing power measurement at the load with the original directional coupler and signal analyzer used in Chapter 3. The coupler used for the feedback path was not designed specifically for 80.5MHz, and so its frequency response also had to be characterized in order to know how the coupled signal was being attenuated.

Following the directional coupler were a passive attenuator, a variable attenuator, and a preamplifier. The passive attenuator and preamplifier were included to help bring the RF feedback signal amplitudes into a range that was more compatible with the dynamic range of the LLRF. The variable attenuator was varied with a control voltage supplied by a signal generator. The control voltage could be setup to enforce a constant attenuation value or one that varied with time. This feature would later be used to emulate microphonics within the test bench setup.

## **4.2 ET Control Algorithm Development**

After assembling the test bench setup, a control algorithm was designed that would work with it. The main factor that would determine the shaping of the control algorithm was the way in which the LLRF operated. The LLRF RF drive signal amplitude depended on the feedback signal amplitude. If the voltage seen at the feedback point varied at all from a user-defined value, the LLRF increased or decreased drive amplitude until the set point was met again. The LLRF was capable of generating RF drive signal amplitudes up to +13dBm; this limit would define the upper limit of operation that would be used in consulting Chapter 3's data tables. The LLRF also had a digital to analog converter (DAC) that could generate a voltage signal whose amplitude depended on the amplitude of the RF drive signal. The DAC signal would be used to control the BOP output voltage.

To create an ET algorithm that maximized efficiency, it was necessary to first consider the drive signal limits of the LLRF. The LLRF could generate drive signals of up to +13dBm. Using this value as a starting point, the data tables were consulted to find the maximum possible efficiency that corresponded to this input power level and the maximum usable supply voltage. The efficiency at +13dBm input power with a 30V supply rail was found to be about 50%. The rest of the data points were selected by working backwards through the tables in order of descending supply voltage and recording the input voltage amplitude that corresponded to efficiency values of about 50% for each supply voltage case. Table 4-1 shows the data collected from the selection process. The minimum allowable supply rail voltage was raised to 14V because it was found that a sinusoidal supply voltage caused oscillation issues when allowed to swing as low as 12V.

Supply Rail Voltage (V)	Input Power (dBm)	Input Voltage ( $V_{pk}$ )	Output Power (W)	Efficiency (%)
14	5	0.56	18.89	51.43
16	6	0.63	24.10	51.90
18	7	0.71	29.85	52.02
20	8	0.79	36.18	52.05
22	9	0.89	42.95	52.21
24	10	1.00	50.00	51.96
26	11	1.12	57.27	51.99
28	12	1.26	64.31	51.50
30	13	1.41	70.68	50.73

*Table 4-1 Characterization data used in ET control algorithm creation*

Plots for comparisons of the selected ET algorithm data points and the DC supply rail voltage cases from Chapter 3 can be seen in Figure 4-2 and Figure 4-3. These plots mimic the principle ET behavior discussed in Chapter 2. Below the 14V threshold, the amplifier would act like a Class A amplifier and its efficiency would vary with output power. Once the output power increases past the threshold limit, the ET algorithm would modulate supply rail voltage and efficiency would be kept almost constant. Though the power amplifier's efficiency will become nearly constant after a certain



point, it can be seen in Figure 4-3 that the gain is no longer constant for all power levels. This linearity issue will actually be corrected by the regulatory action of the LLRF feedback. If this were not the case, it would be possible to instead choose a lower target efficiency for starting point of the ET algorithm; doing so will limit how far into saturation the amplifier will go overall, and the power amplifier gain will become more linear. Since it was known ahead of time that the LLRF would be able to correct for nonlinearity, the aim of the ET algorithm was set for efficiency optimization instead.

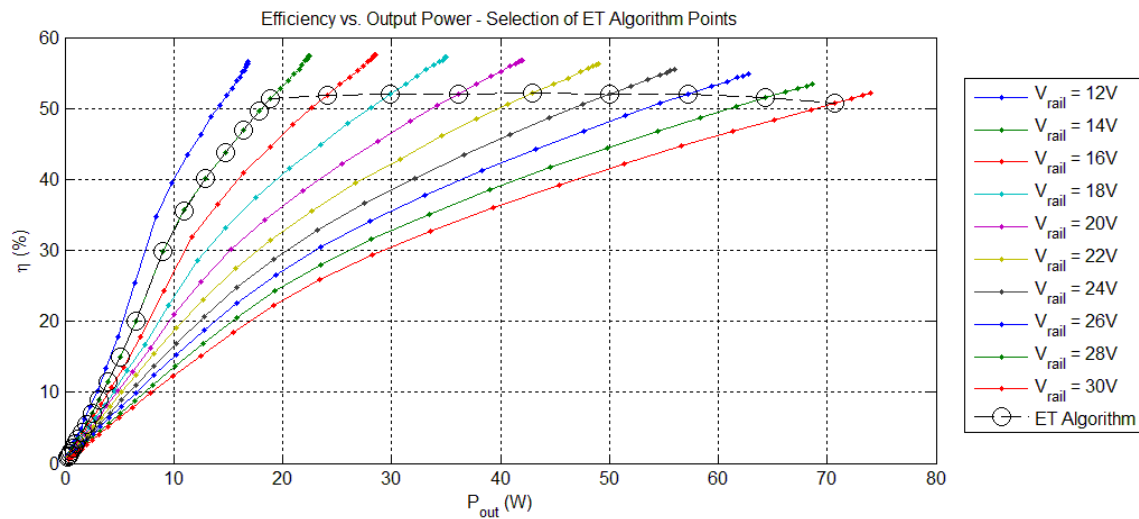


Figure 4-2 Efficiency data points chosen for ET algorithm

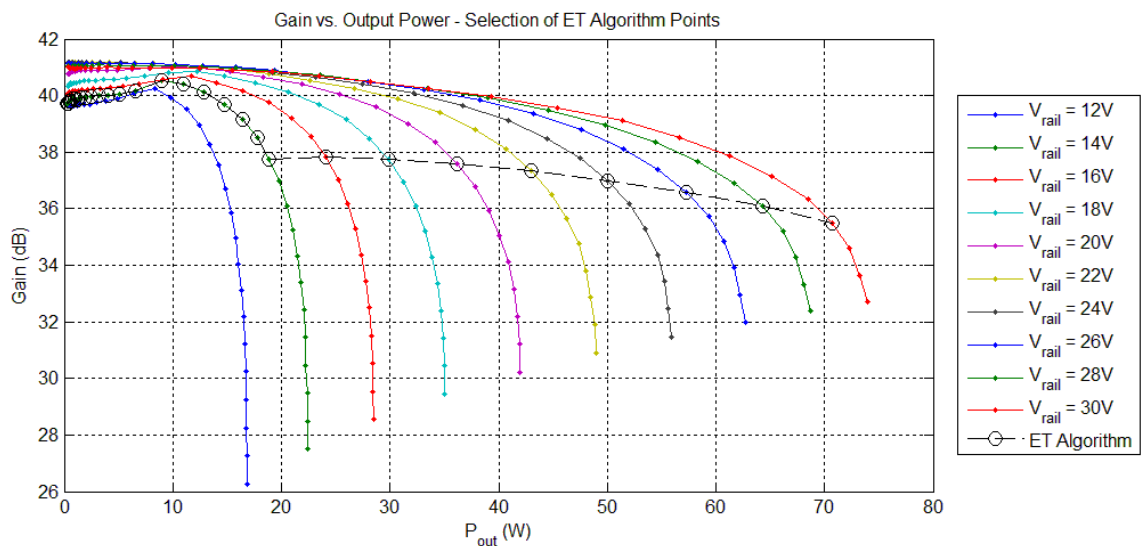


Figure 4-3 Gain data points chosen for ET algorithm

Implementing the control algorithm within the LLRF required that supply rail voltage be related to the voltage amplitude of the RF signal. In order to create the actual algorithm that would be programmed into the LLRF, the rail voltage and input voltage data points were taken from the green columns in Table 4-1 and plotted as shown in Figure 4-4. Using polynomial fitting functions in MATLAB, a line of best fit was created from the voltage data. The resulting equation, also shown in Figure 4-4, was scaled to fit the 0-10V range of the LLRF DAC output and programmed into the LLRF firmware.

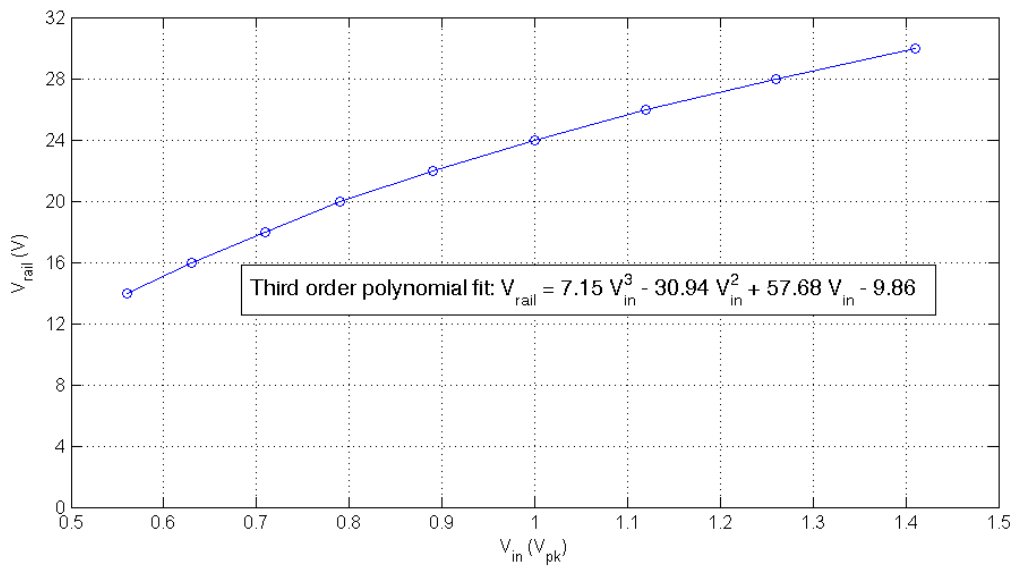


Figure 4-4 ET control algorithm derived from LLRF generated signal amplitude and desired rail voltage

After creating the ET control algorithm, the next task was to verify its operation on the test bench. The ET system would first be tested in a simulation environment without microphonics to verify that the LLRF system was able to implement the algorithm correctly as well as to see the benefits of ET operation with continuous wave signals. Microphonics simulations were then to be introduced into the system to test ET's usefulness under conditions closer to those of the real FRIB environment. These tasks will be covered in the following two chapters.

## CHAPTER 5: ET EXPERIMENTS WITHOUT MICROPHONICS

This chapter will discuss the techniques that were used to verify that the ET control algorithm was working correctly within the confines of the proposed simulation setup. If the algorithm were working correctly, the efficiency measurements for the test bench should be comparable to the data originally used to generate the algorithm. This chapter will also include direct efficiency comparisons between a Class A and an ET system with continuous wave signals.

### 5.1 Experiment Test Setup

A procedure was created to test the control algorithm using the test bench setup that was described in Chapter 4. The procedure was of a similar fashion as the characterization tests used originally in Chapter 3, only now with a few differences. Since the signals in the test bench setup were now being generated by the LLRF system instead of MATLAB-controlled signal generators, a different system had to be used to sweep test parameters. The LLRF was controlled through interactions with the computer-based Experimental Physics and Industrial Control System (EPICS) [27]. EPICS allows users to program the desired set point into the LLRF controller and monitor the feedback response signals. EPICS was used in the tests presented here and in Chapter 6 to control the set point and manipulate the output power level setting.

In order to evaluate efficiency while the amplitude of the RF drive signal was being varied by the LLRF, a MATLAB program was devised that would perform measurements in real time. A flowchart for this code is shown in Figure 5-1, and the script used for the program is presented in Appendix A.3. Once started, the script constantly polled the oscilloscope for BOP voltage and current data and the signal analyzer for output power measurements. The gathered data was used to calculate power supplied to and power output from the power amplifier. Instantaneous efficiency was calculated using the supplied power and output power data and then plotted on a continuously-updating graph.

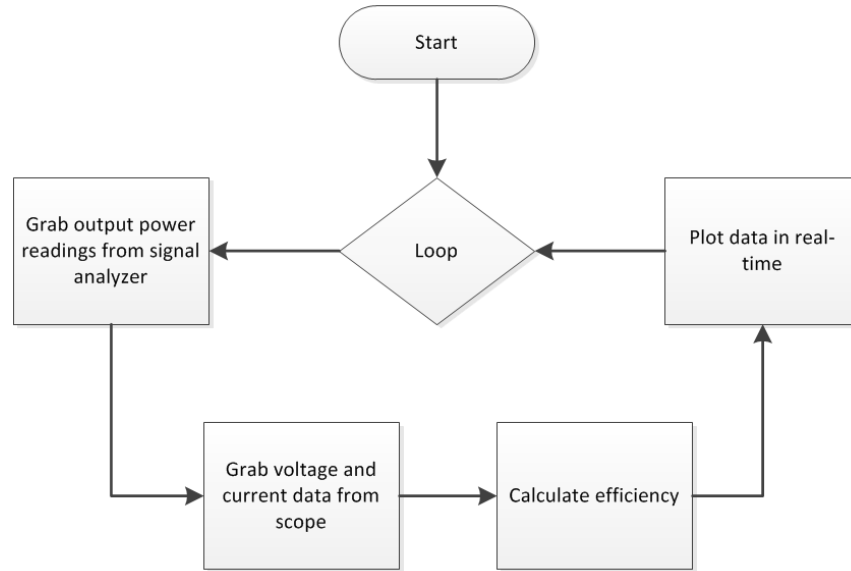


Figure 5-1 Flowchart for live efficiency measurement script

To ensure accurate measurement in a real time environment, several changes had to be made to the way in which the oscilloscope and signal analyzer operated. The signal analyzer had to now be setup to take accurate power measurements quickly, and so would have to have restrictions placed on its span and resolution bandwidth (RBW) settings. To minimize sweep time, a frequency span of 10Hz was used along with a RBW of 1kHz. The center frequency was set at the FRIB target of 80.5MHz. The reduction in measurement span would mean that harmonics of the target frequency would not be able to be measured in this test. The data presented in this thesis focuses mainly on efficiency, but if necessary the THD plots from the characterization tests of Chapter 3 could be used to predict THD performance. In order to synchronize the oscilloscope measurements with the signal analyzer measurements, the signal analyzer's trigger output was connected to the oscilloscope's trigger input.

The procedure for these verification tests was carried out as follows. The supply rail voltage was switched between Class A and ET mode via a toggle switch that routed different signals to the BOP control input. For the Class A mode, a control voltage was chosen that would result in the BOP outputting a constant 30V. For ET mode, the control voltage was set by the LLRF DAC output. The

addition of the toggle switch allowed the experimenter to quickly switch between the two modes. The output power test levels were selected to go from 2.5W to 70W, in 2.5W steps. The output power level was set by adjusting the LLRF set point voltage in EPICS until the desired wattage was arrived at. Efficiency was measured twice for each output power level; once in Class A mode, and once in ET mode. The actual efficiency numbers was gathered by reading off the current reading as recorded by the MATLAB program. After compiling the data, comparisons were made to verify control algorithm functionality and observe ET efficiency gains.

## 5.2 Experimental Results

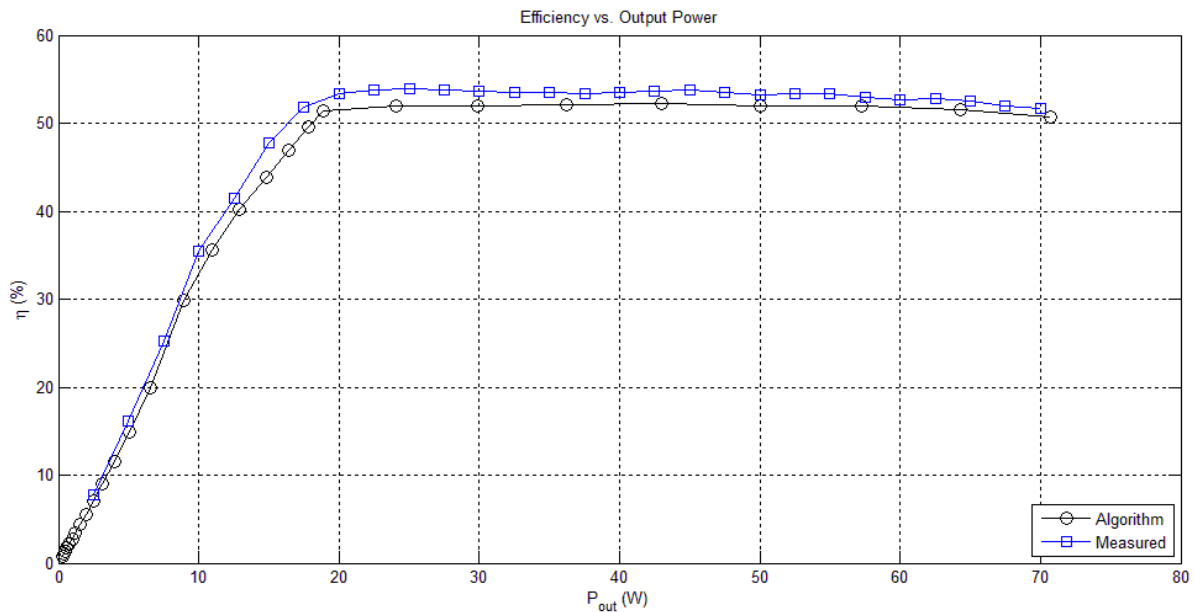


Figure 5-2 Comparison of proposed ET control algorithm and measured performance

The first goal of the experiment was to verify that the algorithm performed as desired. Figure 5-2 shows a comparison between the characterization data points that were selected in Chapter 4 and the actual measured algorithm performance with the LLRF. The first thing to note in the results is that the measured performance has slightly higher efficiency overall than the proposed algorithm. Higher efficiency numbers could be the result of the supply rail voltage being slightly lower than originally

intended. Slight differences in supply rail voltage could have been the result of interpolation error generated by the control algorithm itself, or by the conversion process used by the LLRF to monitor feedback and generate BOP control voltages. The error could also be attributed to the how the data was measured, since the measurement techniques differed slightly between this chapter and the characterization tests from Chapter 3. The difference between measured and proposed performance differed at most by a few percent, and as such the algorithm was deemed operational with the LLRF setup.

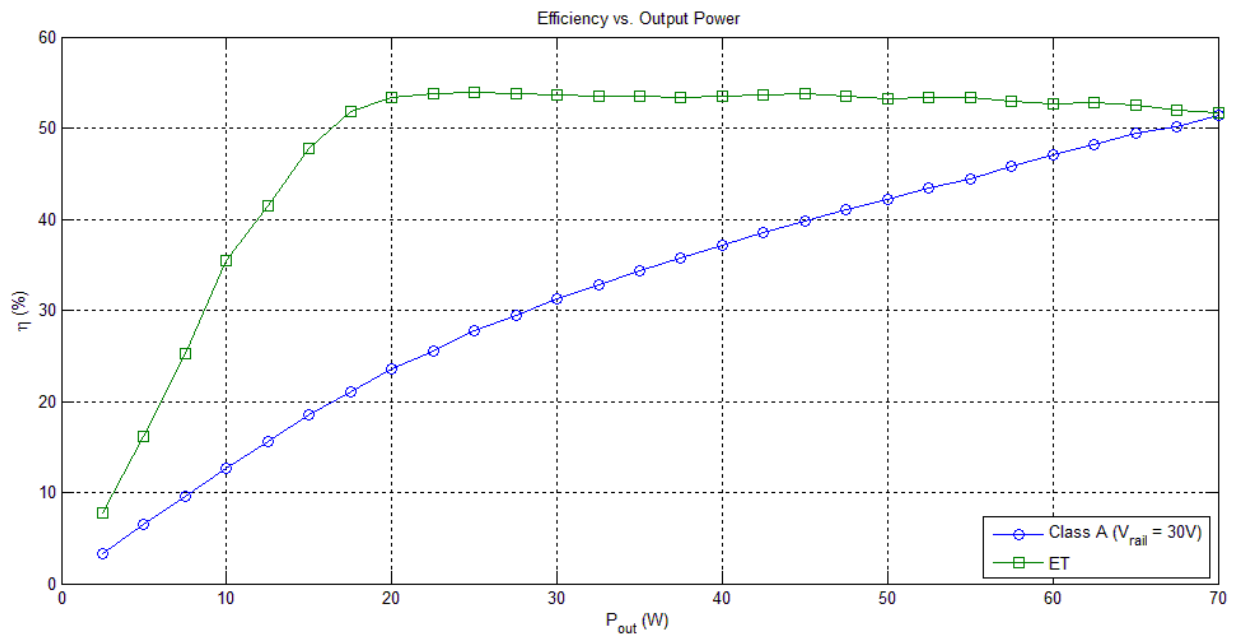


Figure 5-3 Comparison of measured ET and Class A performance

The next task in the analysis was to compare the results of the experiment when operating in a Class A mode and when operating with ET activated. A comparison of the measured efficiency for Class A and ET systems is shown in Figure 5-3. When operating under ET, the power amplifier has greater overall efficiency than when in Class A. The ET system is also able to maintain a nearly constant efficiency level at higher power levels, while the Class A system has efficiency that varies with power. A more helpful visualization is shown in Figure 5-4, where the difference in efficiency between Class A and

ET has been plotted with respect to output power. When operating under ET, the power amplifier is at most 30% more efficient than if it was operating as a Class A device. The two systems have nearly the same efficiency at 70W because at that point both the ET and Class A supply rail is set to 30V.

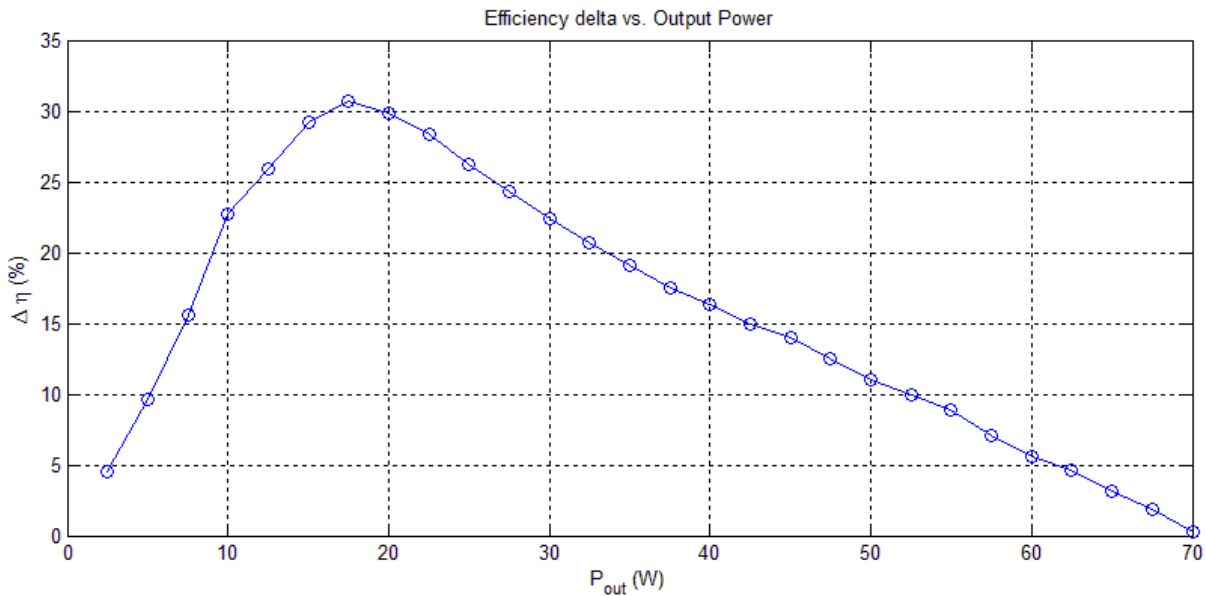


Figure 5-4 Efficiency difference between measured ET and Class A performance

To illustrate the improvements gained by the ET system and to showcase the actual functioning of the MATLAB script used, three points of interest were selected for real-time comparison of Class A and ET efficiency. Each of the plots captured the change in efficiency as the system was switched from Class A to ET. The first comparison focused on the difference in efficiency at 10W, when the output power level was below the control algorithm threshold and the ET supply rail voltage was held at 14V. The second comparison highlighted the point where the efficiency difference was at its greatest, at 17.5W. The third comparison took a look at 70W, where Class A and ET had nearly the same efficiency. The data points that were chosen for analysis can be seen in Figure 5-5.

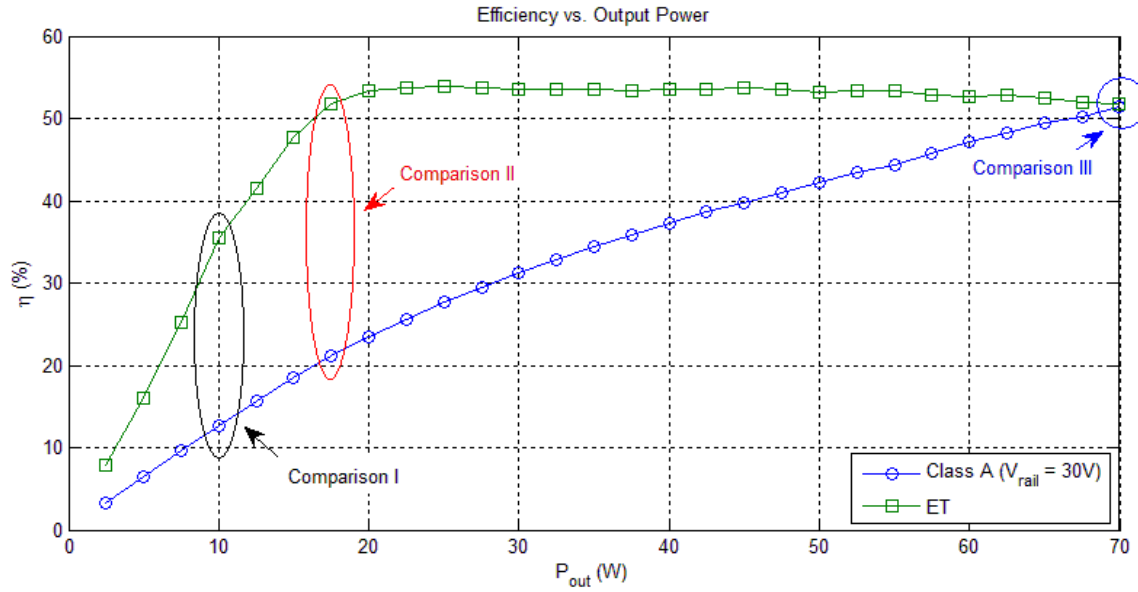


Figure 5-5 Points of comparison chosen for real-time analysis

Plots from the real-time MATLAB experiments are shown in Figure 5-6, Figure 5-7, and Figure 5-8. These plots show power amplifier efficiency as a function of time instead of output power. The MATLAB script functioned by plotting the most recent data point at the right side of the plot. As more data was recorded, the older data points would scroll to the left side of the plot until they were no longer a part of the time window. The length of the time window for the plots shown here was set to 35 seconds. It was typical during testing to start up the measurement script once and then leave it running while a multitude of tests were performed.

While running the MATLAB script, the most recent supply rail voltage, output power, and efficiency measurements were updated continuously in the plot's legend in the upper right corner. In the first half of each figure, the efficiency is shown for the power amplifier operating as a Class A device. In the middle of each plot, a discontinuity can be seen where the power amplifier was switched from Class A to ET mode by the experimenter.



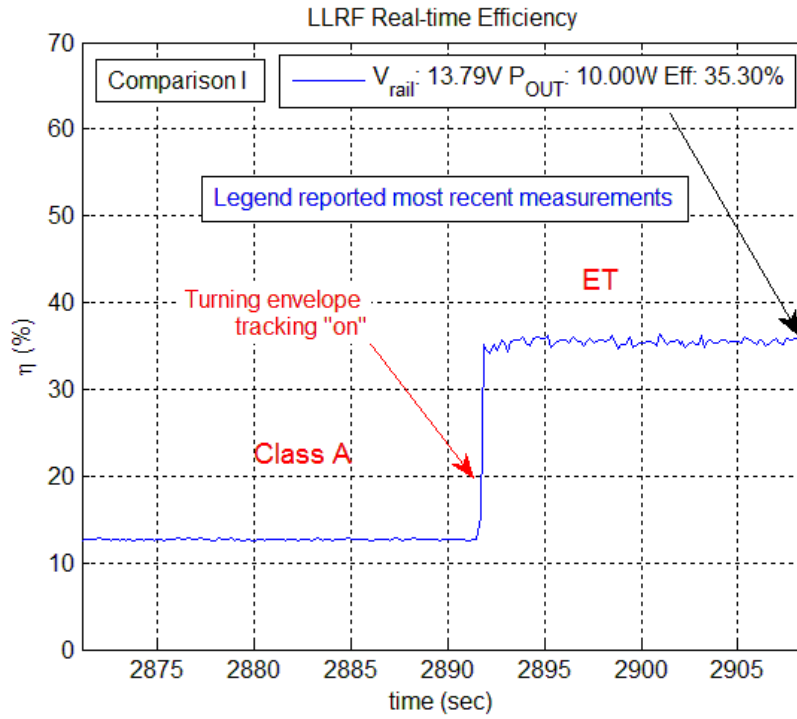


Figure 5-6 Real-time measurement of efficiency for ET and Class A, first comparison

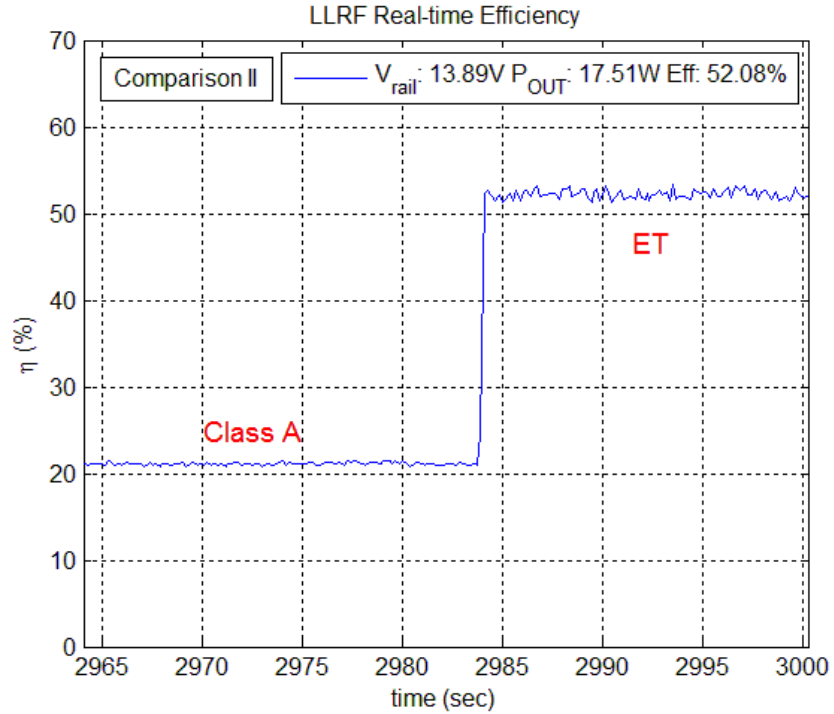


Figure 5-7 Real-time measurement of efficiency for ET and Class A, second comparison

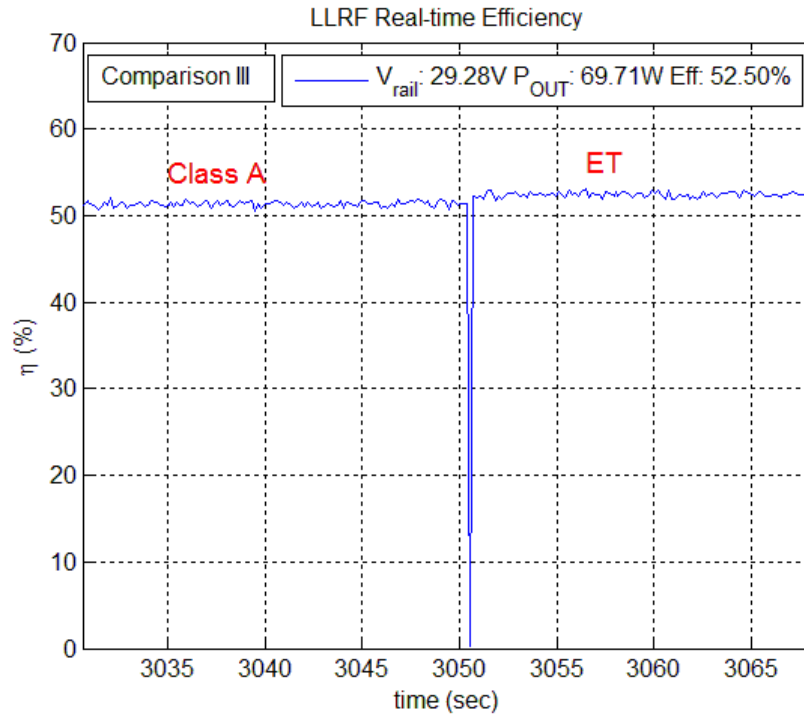


Figure 5-8 Real-time measurement of efficiency for ET and Class A, third comparison

The results presented in this chapter proved that implementing the ET algorithm did show substantial improvements in efficiency for ideal cases where no microphonics were present. This was done mostly to provide some initial verification of ET test bench operation. Although this was useful as an initial test run, this was not the most practical usage. The real FRIB cavity environment will have microphonics present that will cause the amount of required output power to fluctuate. The next chapter will take the test bench setup used here and add modulation of the RF feedback signal in order to simulate microphonics. Introducing microphonics into the test bench experiments would help garner data for a more practical assessment of a FRIB ET implementation.

## CHAPTER 6: ET EXPERIMENTS WITH MICROPHONICS

The last experiments performed with the ET test bench observed efficiency performance while simple simulations of microphonics were introduced into the system. Because of the fact that the test bench was created from equipment that was available at FRIB, some compromises had to be made to achieve greater accuracy or avoid instability. Despite the concessions that had to be made, the results of these tests still offer insight to the operation of an ET system.

### 6.1 Experiment Test Setup

In order to simulate microphonics in the ET test bench system, the variable attenuator's control signal was changed from a DC voltage to a sinusoidal voltage. The LLRF sensed changes in feedback amplitude and adjusted its RF drive amplitude to compensate. Although a sine wave was chosen to act as the control voltage for its simplicity, a more accurate simulation would instead use a much noisier signal such as the real-world data shown in Chapter 1. The real interest of this chapter's experiments was to observe how the ET test bench setup would react to an amplitude-modulated RF signal.

A test was devised to compare the efficiency performance of ET and Class A with microphonics applied to the test bench setup. Using the live efficiency measurement MATLAB script from the previous chapter, the drain efficiency of the amplifier would be observed for a predetermined output power swing. The variable attenuator control voltage swing was selected such that it would vary the attenuation factor over a 3dB range. The control range was chosen from a mostly-linear part of the attenuation curve, so that a linearly-varying control voltage would result in a linearly-varying attenuation factor. The 3dB attenuation range was chosen in order to fulfill the output power variance design requirement mentioned in Chapter 1. The LLRF feedback set point voltage would be altered to set the minimum value of this swing.

The main goal of these experiments was to determine if the ET test bench system could perform as it should with a RF signal of varying envelope. According to the principles discussed in Chapter 2, there are three main regions of operation with ET. In the first region, the power amplifier operates at low power levels and the ET algorithm will hold the supply voltage constant. A second region exists as the output power increases and the ET algorithm modulates the supply rail voltage at signal peaks. The third region consists of full supply rail modulation at high output power levels. These three regions were selected from the range of output power available from the power amplifier, as shown in Figure 6-1.

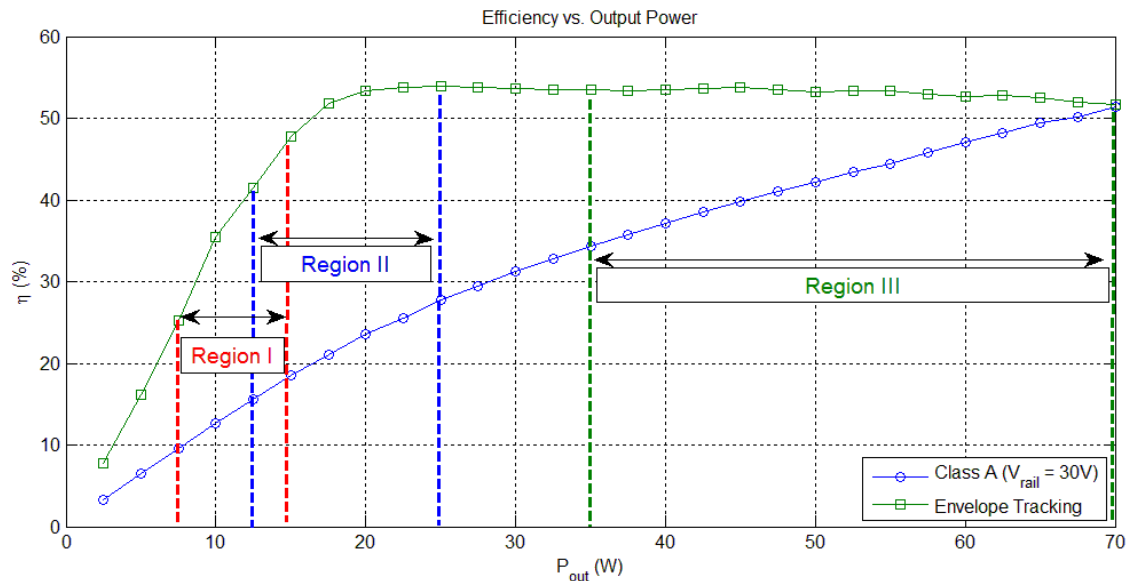


Figure 6-1 Regions of operation chosen for comparison of ET and Class A

## 6.2 Experimental Results

The real-time efficiency measurements for the first region of operation are shown in Figure 6-2. The efficiency data was taken as a snapshot from the constantly-updating plot being generated by the real-time measurement MATLAB script. As with the real-time efficiency measurements shown in Chapter 5, these plots show the efficiency of power amplifier acting in Class A on the left half, and then in ET on the right hand side. Illustrations of the supply rail voltage and output power have been

supplied with the real-time efficiency measurements to aid the analysis. The supply rail voltage for the Class A sections was fixed at 30V for each region.

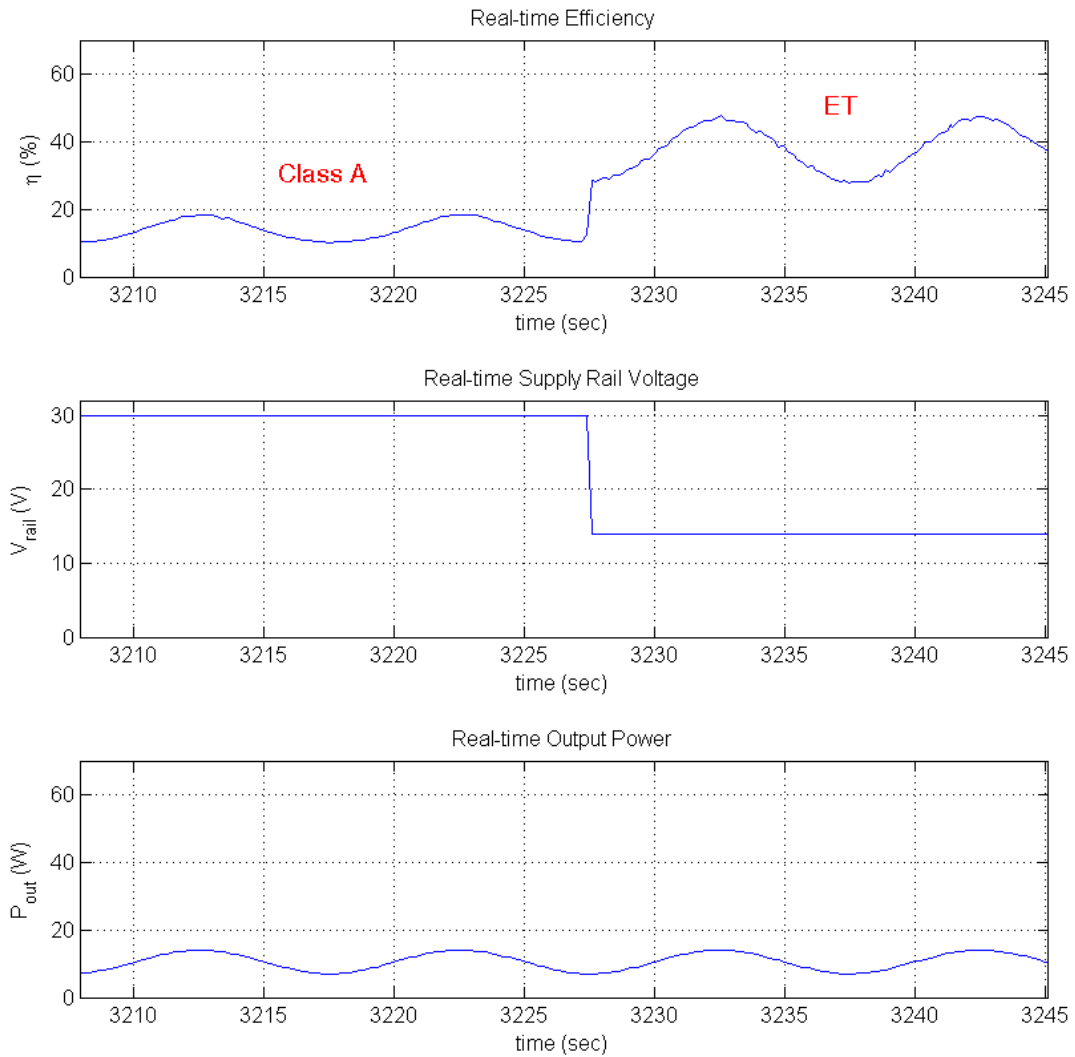


Figure 6-2 Region I real-time efficiency data, with illustrations of supply rail voltage and output power

In the first region of operation, the output power swing was adjusted to go between 7W and 14W. The ET supply rail voltage was fixed at 14V at this point because the output signal was not large enough to exceed the threshold determined by the control algorithm. Both Class A and ET had fixed supply voltages in the first region, and therefore both have efficiency that varies with output power

swing. The difference between output voltage and supply voltage is much lower at 14V, resulting in a higher overall efficiency with ET engaged.

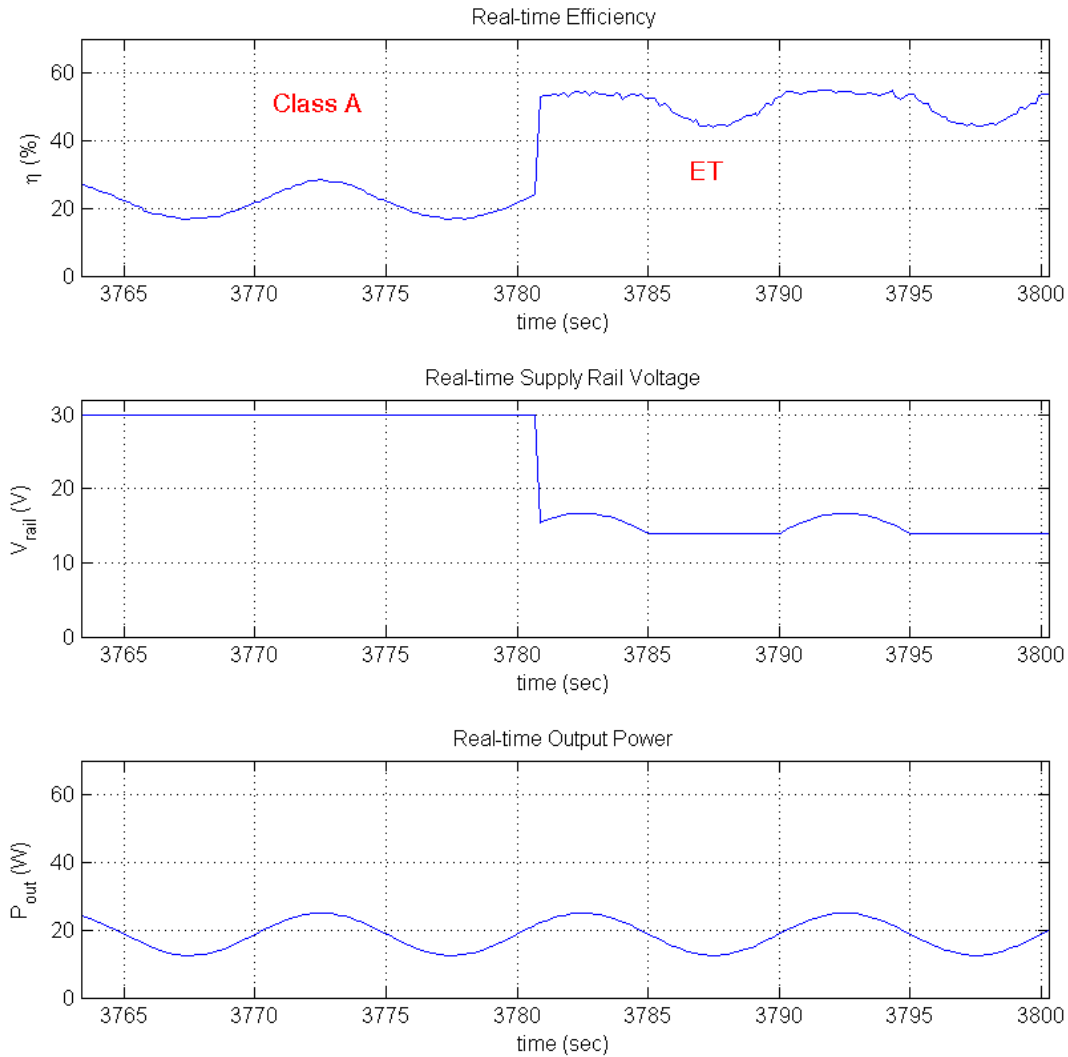


Figure 6-3 Real-time efficiency data for Region II comparison

The second region compared efficiency results for output power between 12.5W and 25W. The results for the second region are shown in Figure 6-3. The efficiency of the power amplifier with ET engaged can be seen to be nearly constant when the output signal is at its peak. This is because the difference between supply rail voltage and output voltage are kept constant by the tracking action of the control algorithm. As the output voltage drops below the threshold set by the control algorithm, the

supply rail voltage is set to a constant value and efficiency again varies with signal swing. The efficiency for the Class A portion of this data is higher than the Class A results from the previous region, but is still much lower than the efficiency with ET engaged.

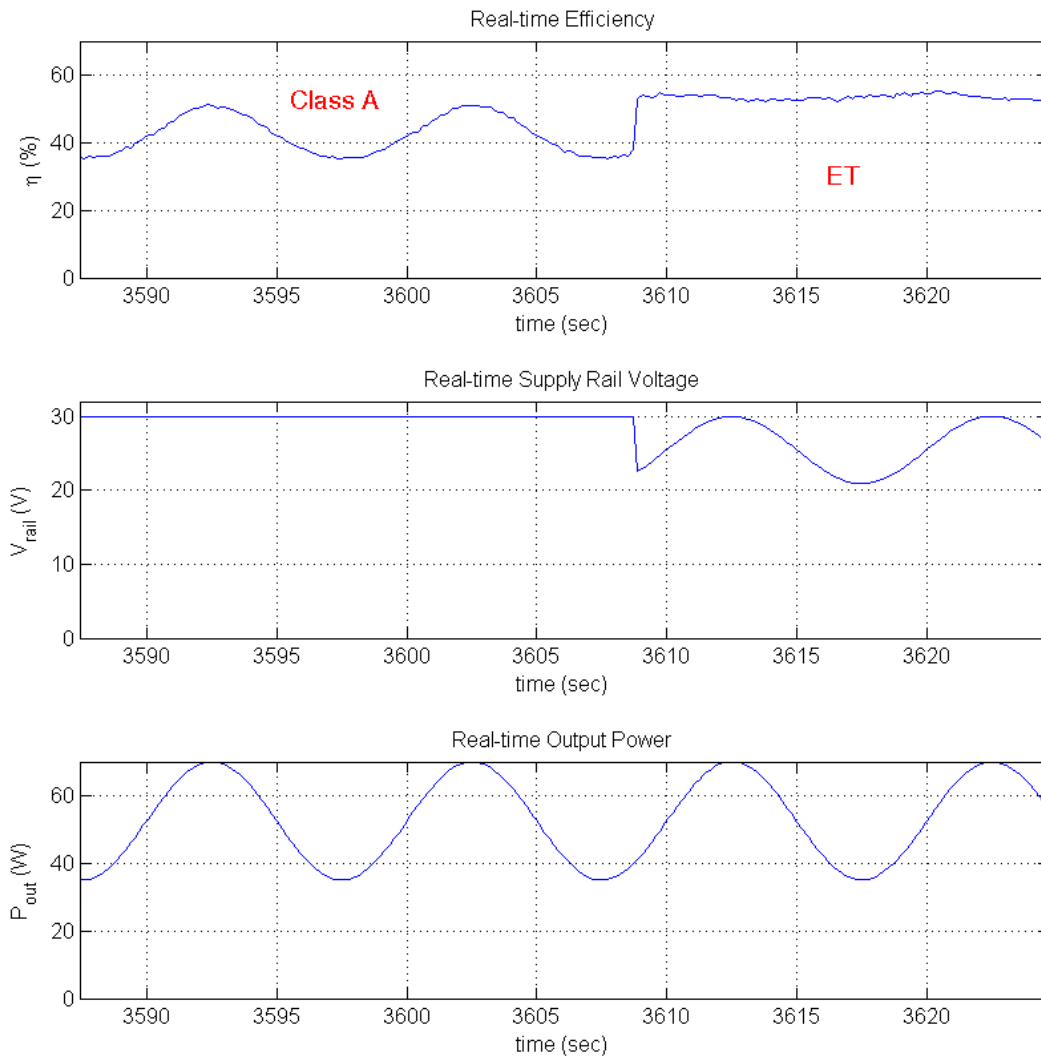


Figure 6-4 Real-time efficiency data for Region III comparison

The third region looks at efficiency as output power swings between 35W and 70W. The measurements taken for the third region are shown in Figure 6-4. The efficiency in this higher power region is nearly constant for the entirety of the signal swing when ET is engaged. This is because the whole swing of the signal exceeds the algorithm threshold, and so the control algorithm always tracks

the output voltage with the supply rail voltage. It is also in this region that Class A shows relatively high efficiency numbers, and in fact the efficiency of both systems are nearly the same at the peaks of the output swing. The efficiency numbers for Class A and ET intersect in the third region because the supply rail voltage peaks at 30V when ET is engaged; the same voltage that the Class A supply rail is set at.

	Region I		Region II		Region III	
	Class A	ET	Class A	ET	Class A	ET
<b>Min (%)</b>	10.12	27.77	16.79	43.65	35.16	52.20
<b>Max (%)</b>	18.45	47.64	28.58	55.02	51.19	55.13
<b>Mean (%)</b>	13.90	38.12	21.40	50.60	42.02	53.46
<b><math>\Delta</math> Mean (%)</b>	<b>24.22</b>		<b>29.20</b>		<b>11.44</b>	

Table 6-1 Comparison of efficiency between Class A and ET

A summary of the minimum, maximum, and average recorded efficiency results are shown in Table 6-1. A calculation for the average efficiency difference between Class A and ET has also been included for each region. It is possible to see from these results that ET can offer excellent gains in average efficiency over Class A, especially in the second region.

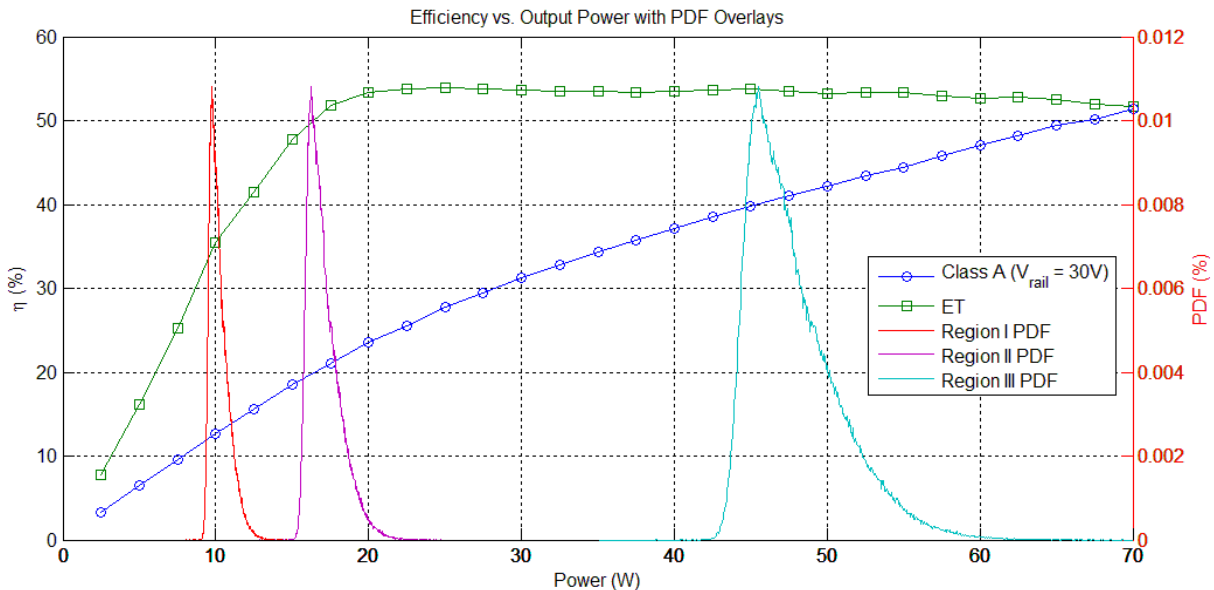


Figure 6-5 Efficiency curves with PDF overlays



Despite the fact that Gaussian noise was not used to simulate microphonics in these tests, the data gathered could still be used to predict average ET efficiency gains. Average efficiency gains can be predicted with the use of the PDF data from Chapter 1. This PDF was created from forward power measurements that were taken from another cavity system. If the PDF is scaled down to the power levels used in these experiments, some insight can be gained on how much ET would improve a system with real microphonics. Figure 6-5 shows the PDF from Chapter 1 superimposed over each of the three regions of interest that were presented in this chapter. The peak of each PDF occurs at the average power level for that region. A summary of estimates for the average efficiency gains made in each region are shown in Table 6-2. These results show that the efficiency gains to be had in each of the regions are actually fairly close to those reported in Table 6-1, with some improvement shown in the third region.

	<b>Region I</b>	<b>Region II</b>	<b>Region III</b>
<b>P<sub>average</sub> (W)</b>	10	17	45
<b>Δ η (%)</b>	22.7	30	14

*Table 6-2 Predicted average efficiency gains for PDF overlays*

The energy savings estimates from Chapter 1 stated that if efficiency for the RF systems could be improved by 15%, it would be possible to save over a quarter of a million dollars a year. The results from Table 6-2 show that the ET test bench was capable of meeting this requirement for much of the power amplifier's output power range. For the third region of operation, the ET efficiency improvement estimate is 1% under the FRIB requirement. Considering the fact that not all of the FRIB experiments will require operation at the extreme end of the RF amplifier output power capabilities, this discrepancy could be considered a minor detail.

### 6.3 Issues with Experimental Setup

Some challenges were encountered in the effort of changing the test setup to include microphonics. The LLRF was originally designed for systems that had a super conducting cavity for a load. The cavities were designed to have extremely high Q and therefore have operating bandwidths on the order of tens of Hertz. It is possible to tune the LLRF to work properly with systems such as the one presented in this chapter, however this was not carried out as it was not considered worthwhile to tune the LLRF to work with a test bench system that was vastly different than the LLRF's normal conditions.

The system used in these experiments was vastly different than the LLRF's original intended application mainly because of its bandwidth. The bandwidth of a system is limited to that of the component with the narrowest bandwidth. This meant that the cavity bandwidth would determine the overall bandwidth in the original application, since other components had much wider operating bandwidths by comparison. The load used in the test bench experiments was not a high-Q cavity but instead a wideband 50Ω resistor, meaning that the system bandwidth was determined by one of the other components. A likely candidate for lowest bandwidth in the ET test bench was the power amplifier, whose specifications listed an operating bandwidth of 33MHz [24]. Compared with a normal cavity bandwidth on the order of tens of Hertz, it is easy to see why there would have been issues adapting the LLRF to the ET test bench.

The disparity between the original cavity system bandwidth and the test bench system bandwidth would prove to cause problems in selecting a test frequency to simulate microphonics with. This problem can be seen when comparing the feedback set point voltage for different microphonics frequencies, as shown in Figure 6-6 via the EPICS monitoring software. The set point voltage can be seen to stay constant for very low frequency microphonics on the left side of the plot. As the microphonics frequency increases, the set point voltage can be seen to oscillate slightly around the

desired set point voltage. If the microphonics frequency is increased further, the LLRF will eventually lose all capacity for control and the set point voltage will vary wildly. These oscillations are artifacts of the drastic change in system bandwidth. It was decided that it would be best to maximize stability in the system and opt for lower frequency performance.

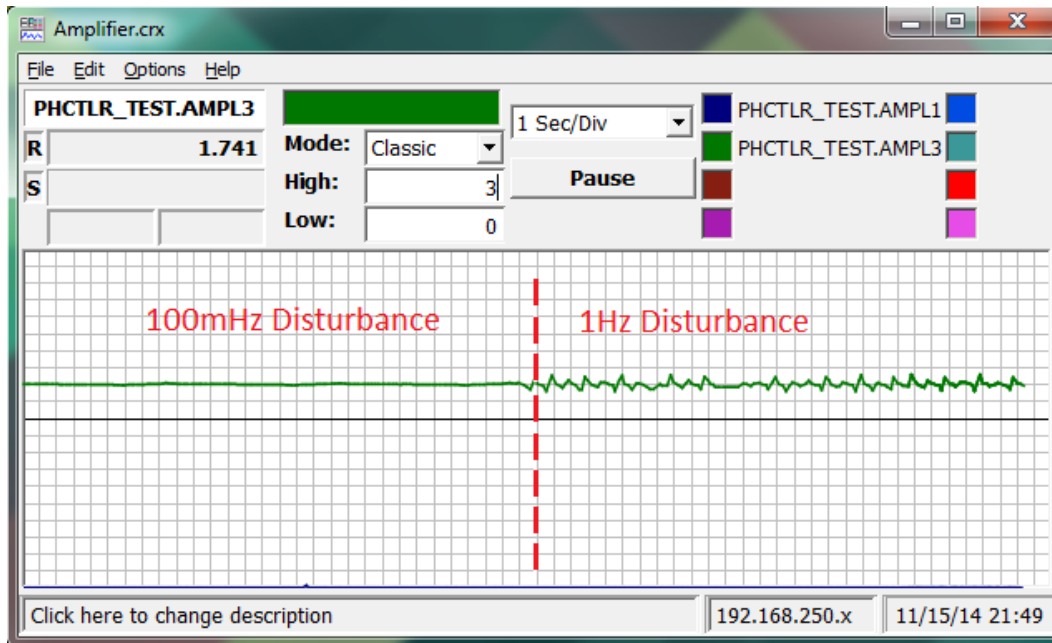


Figure 6-6 Loss of regulation in LLRF system

Despite the difficulties involved in integrating the LLRF into the test bench system, it was still possible to pull useful results from the experiments performed here. With the simple case of sinusoidal microphonics, the tests presented here were able to demonstrate the ET operation principles detailed in Chapter 2. The ET test bench setup did indeed showcase great gains in efficiency when compared to the more traditional Class A system, and with proper tuning the test bench system could very well duplicate these results for bandwidths more in line with FRIB requirements.

## CHAPTER 7: CONCLUSION

The aim of this thesis was to investigate the efficiency gains that an ET system had to offer when used in an environment similar to the one the actual FRIB RF amplifiers would be exposed to. Once FRIB is completed, it will be the responsibility of the RF amplifiers to maintain the electric field strength within the superconducting cavities. The RF amplifiers will have to compensate for cavity detuning due to microphonics, which will in turn mean that the amplifiers will have to operate over a range of output power. Because FRIB needs many cavities to operate, the power consumed by the RF amplifiers that drive them will be of considerable magnitude. ET technology was chosen as a candidate for investigation because it was purported to offer substantial efficiency improvements over classical amplifiers with DC supply voltages, especially in applications that require varying amounts of output power. The work presented in this thesis attempted to show that ET was indeed worthy of implementation by constructing a scaled-down test bench version of the FRIB cavity drive problem.

The first step in assembling the ET test bench was to characterize the power amplifier that would be used in all of the ET tests. The characterization tests recorded efficiency, gain, and THD of the power amplifier while input power and supply rail voltage were varied. The results that were gathered verified that a high degree of linearity and high efficiency are mutually exclusive for RF amplifiers with DC supply voltages.

Following characterization was the creation of the ET algorithm. The algorithm enabled the supply voltage to closely follow the envelope of the power amplifier's output, thereby optimizing efficiency. To create the algorithm, a sample set of optimum efficiency data was first taken from the characterization tables. Polynomial curve fitting was then used to generate an equation that related supply voltage to input signal amplitude. The equation had to be related to input signal amplitude

because of the capabilities of the LLRF control system that would be used to run the ET test bench experiments.

After a control algorithm had been created, it was possible to do the initial ET test bench experiments. The first round of tests focused on the ET system's ability to deal with continuous wave signals. These tests were also the first to draw definite comparisons between ET and Class A. A MATLAB script that measured efficiency data in real-time had to be implemented in order to work with the separate LLRF system. The test results showed that ET operation offered great improvements in efficiency when compared to Class A, especially when operating at low output power.

The last batch of tests would introduce microphonics into the test bench setup to better approximate the conditions the ET system would experience if installed in FRIB. The microphonics used here consisted of a simple sine wave that resulted in a 3dB modulation of output power. The original power savings calculations done for the FRIB RF systems estimated that over a quarter of a million dollars could be saved each year if the overall average efficiency could be increased 15%. Using scaled down versions of real cavity power PDFs, it was determined that the ET system could indeed meet and even exceed these numbers given the right conditions.

Problems were encountered in setting the frequency of the microphonics signal to anything above 1Hz. The root of the problem lay in the fact that the bandwidth of the test bench system was much larger than what the LLRF was programmed for. This could have been rectified by tuning the LLRF specifically for the test bench, but this was less than practical because of the possibility that the LLRF module would need to be used for experiments elsewhere in the facility. Another possibility would have been to design a band-pass filter to bring the bandwidth of the ET system down to more reasonable levels for the LLRF. With the test bench system and LLRF in tune, it should be possible to see ET operate correctly for a much wider bandwidth.

## 7.1 Practical Considerations for ET

Because of the specificity of the experiments presented in this thesis, some aspects of ET system design were not explored as thoroughly as others. A list of practical ET design considerations will be given here in the interest of aiding future design. The main purpose of the FRIB ET test bench was to investigate relative efficiency improvements, rather than overall efficiency for an ET system. Because of this, only the drain efficiency of the power amplifier was measured. For instances where total system efficiency is desired, the efficiency of the power supply must be included. Inclusion of power supply efficiency can add more complexity to the measurement procedure, since the efficiency of the supply itself will also vary with output power.

Choosing a proper power supply for use in an ET system can be very important. The power supply should be able to maintain stability for the full voltage range and modulation bandwidth. The power supply should also be as linear as possible for the signals of interest, as distortion in the supply voltage waveform could carry over to distortion of the output signal.

Modification of the power amplifier circuitry may be necessary in order to properly integrate it into an ET system. For power amplifiers that are normally used with DC supply rail voltages, the cutoff frequency of the supply rail circuitry will most likely have to be increased to include the bandwidth of interest for supply modulation. Care must be taken when doing this so as to avoid issues such as increased power supply noise and possible instability of the RF amplifier.

It is also necessary to assess the actual cost of an ET system before implementing it. Developing a working ET system may end up taking up a considerable amount of time and money when compared to installing standardized DC supply systems. The increased complexity of the ET system can also result in more downtime and higher costs for repair. The main attraction of the ET implementation is that it

will end up saving more money in future energy costs. The costs of repair and development for an ET system should be weighed against its prospective energy savings before finalizing realization.

## 7.2 Future Work

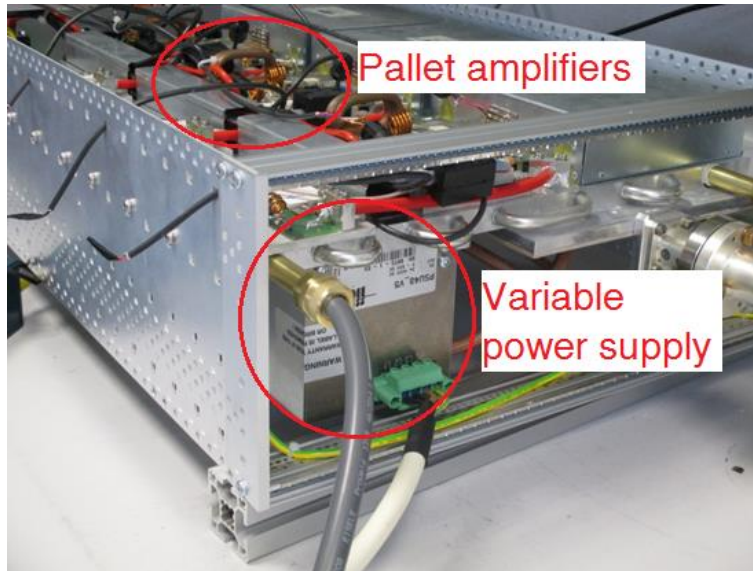


Figure 7-1 HBH ET RF amplifier prototype<sup>4</sup>

The implementation of ET RF amplifiers is already underway. A production contract was recently awarded to HBH Microwave GmbH [28] to design high power RF amplifiers capable of handling ET operation. The amplifiers will be designed to accept a 0-10V signal from the LLRF for supply voltage modulation purposes. Once completed, the ET system will be able to handle a modulation bandwidth from 30 – 3kHz. A picture of a current prototype model is shown in Figure 7-1.

Work is still being done to integrate the pallet amplifier sections with the variable power supply. Part of this work included characterizing the variable power supply under a range of load conditions. Figure 7-2 shows the efficiency range of the power supply for several DC voltage settings. From this data, it can be gathered that the power supply maintains nearly constant efficiency for higher voltage settings and larger power draw. As the amount of power required from the supply drops, so too does

---

<sup>4</sup> Used with permission from HBH Microwave GmbH ([www.hbhmw.de](http://www.hbhmw.de))

the power supply's efficiency. This will not likely be an issue as the FRIB experiments will require operation over a wide range of power, and the low efficiency range is relatively small compared that of high efficiency.

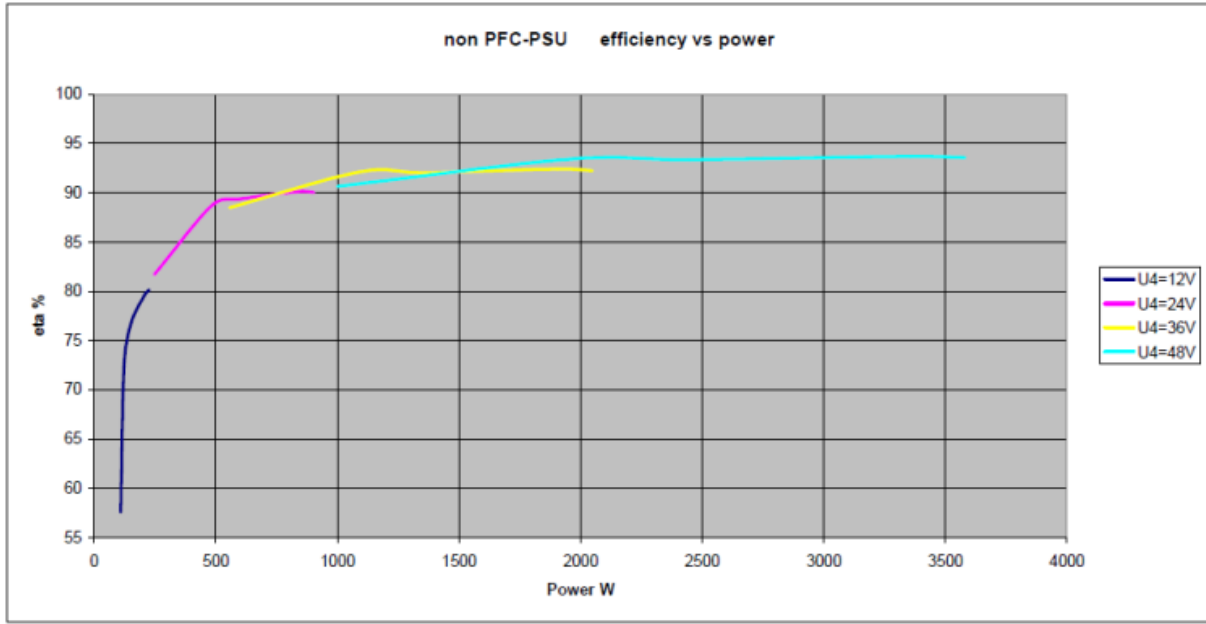


Figure 7-2 Efficiency of FRIB prototype power supply for various loads and supply voltage settings<sup>5</sup>

Tests have also been carried out that verified the performance of the power supply with variable control signals. Figure 7-3 shows oscilloscope measurements of the power supply. The yellow trace at the top of the screen was the 0-10V control signal, the blue trace shows power supply output voltage, and the green trace shows the current drawn from a resistive load. Power supply stability was verified for signals ranging from 30 – 3kHz and with output voltage swings from 10 – 50V.

<sup>5</sup> Used with permission from HBH Microwave GmbH ([www.hbhmw.de](http://www.hbhmw.de))



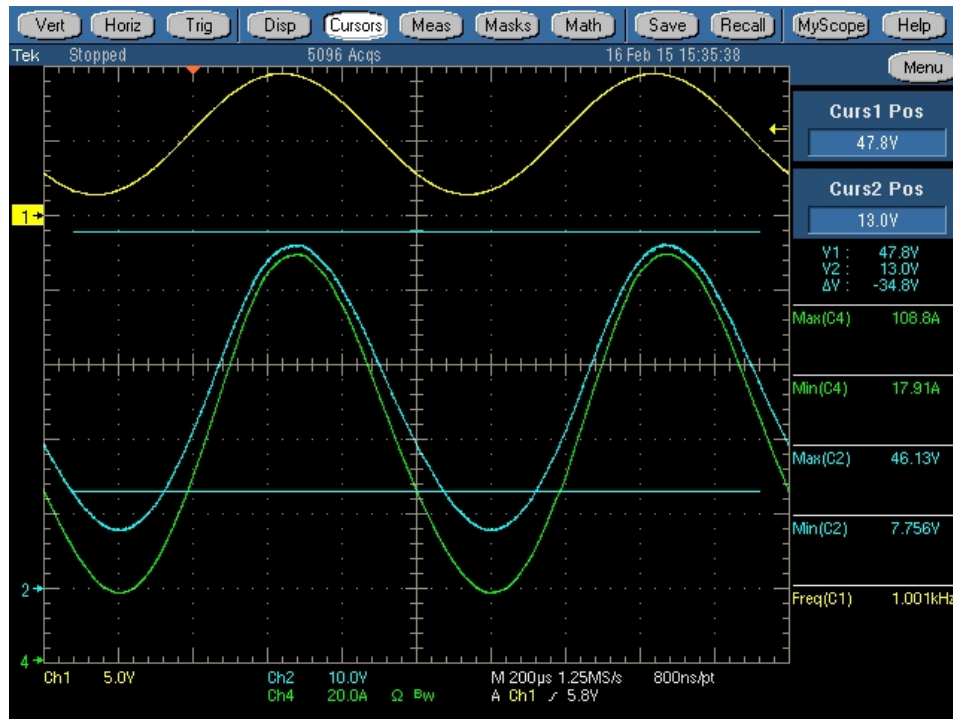


Figure 7-3 Variable power supply waveforms for 1kHz modulation<sup>6</sup>

<sup>6</sup> Used with permission from HBH Microwave GmbH ([www.hbhmw.de](http://www.hbhmw.de))

## **APPENDIX**

## A.1 Permission for Reusing Copyrighted Photos

**Larter, Tom**

---

**From:** King, Karen  
**Sent:** Friday, November 07, 2014 9:45 AM  
**To:** Russo, Thomas; Larter, Tom  
**Cc:** Morris, Dan  
**Subject:** RE: Using FRIB material in thesis

Hello Tom,  
I chatted briefly with Thomas about this yesterday. Permission is granted to use the images and they should be credited to Michigan State University.

Thank you,  
Karen

---

**From:** Russo, Thomas  
**Sent:** Wednesday, November 05, 2014 11:00 AM  
**To:** Larter, Tom; King, Karen  
**Cc:** Morris, Dan  
**Subject:** RE: Using FRIB material in thesis

Hi Karen,

As discussed, Tom Larter would like to use a few FRIB images as part of his thesis. These images include RF cavities, the FRIB tunnel layout, and chart of the nuclides. Tom will need to:

1. Obtain permission to use the images
2. Properly give credit to the source of the images.

Can you let us know what we need to do?

Thank you.

Tom

---

**From:** Larter, Tom  
**Sent:** Wednesday, November 05, 2014 10:35 AM  
**To:** Russo, Thomas  
**Cc:** Morris, Dan  
**Subject:** Using FRIB material in thesis

Hi Tom,

Do you have any idea who I could talk to about getting permission to use FRIB diagrams in my thesis?

Thanks,

**Tom Larter**  
Graduate Research Assistant  
Facility for Rare Isotope Beams  
640 South Shaw Lane

## A.2 Pallet Amplifier Characterization Test Automation Code

```
%% Written by Tom Larter
% This program connects to multiple instruments and uses them to perform DC
% bias sweeps on pallet amplifiers and plot gain compression, efficiency,
% and power gain.
%
% Bench setup:
%   Scope:
%     - Ch 1 on BOP remote out voltage on LLRF box
%     - Ch 2 on BOP remote out current on LLRF box
%     - Ch 4 connected to Signal Analyzer trigger out on back of analyzer
%     - Uses save state "2"
%
%   Signal Analyzer:
%     - Connect 40dB coupler to input through 20dB attenuator
%     - Uses save state "Class H Pallet Amp Wideband sans coupler.state"
%
%   LF Signal Generator (Address: GPIB-10):
%     - Connect output to Sig Gen remote input on LLRF box
%
%   HF Signal Generator:
%     - Connect to input of ZHL-1A preamp
%
%   BOP:
%     - Connect Dsub 9 connector to back of LLRF box
%     - Connect front panel output to PA with a banana-CPC cable
%     - Connect front panel negative output to ground
%
%   Preamp:
%     - Connect output to input of power amplifier
%     - Make sure that 24V connection is hooked up to terminal strip and
%     that the 24V PS is switched on (fan attached to underside of rack
%     mount should come on)
%
%   Power amp:
%     - Connect output to input of 40dB output coupler
%
%   Coupler:
%     - Connect high power output to 50 Ohm load rated for 100W or
%     greater.
%     - Connect reverse coupling to a 50 Ohm load.
%
% LLRF Box settings:
%     - Gain range switch set to "x5", BOP gain knob should be tuned so that
%     a remote input of -5V results in a BOP output of 18V
%     - MOD SEL should be flipped down so that the red "SG" indicator LED
%     lights up
%
% Output syntax:
% [poutW,pindBm,pinW,pdissW,eff,gain,thd,vData,iData,group] = palletDC
%
% Written 7/24/2014

function [poutW,pindBm,pinW,pdissW,eff,gain,thd,vData,iData,group] = palletDC
```

```

%% House keeping
format shortEng; clc;

% System constants
global rfFreq vScale iScale preGain rfPwr railVdc warmTime mkrNum bopDC
rfFreq = 80.5; %[MHz] CW frequency
vScale = 3.6; %[Unitless] Remote V scaling (adjustable)
iScale = 1.2; %[Unitless] Remote I scaling
preGain = 17.2; %[Unitless] ZHL-1A preamp gain
rfPwr = -20.; %[dBm] Initial input power setting for instConfig
railVdc = 28; %[V] Initial rail voltage setting for instConfig
warmTime = 1; %[seconds] For amplifier warm-up time
mkrNum = 6; %[Unitless] Number of signal analyzer markers
bopDC = -railVdc/vScale; %[V] Actual programming voltage value

% System parameters
global vDCMin vDCStep vDCMax vDCSize pinMin pinStep pinMax pinSize cplErr
vDCMin = 12; %[V] Rail voltage sweep minimum
vDCStep = 2; %[V] Rail voltage step
vDCMax = 30; %[V] Rail voltage sweep maximum

pinMin = -32.2; %[dBm] Input power sweep minimum
pinStep = 1; %[dBm] Input power step
pinMax = -1.20; %[dBm] Input power sweep maximum

vDCSize = size(vDCMin:vDCStep:vDCMax,2); %[Unitless] Used for
preallocation
pinSize = size(pinMin:pinStep:pinMax,2); %[Unitless] Used for
preallocation
cplErr = [40,34,30.55,28.16,26.33,24.87]; %[dB] Coupler correction

% Check test readiness before running
fprintf('Before running palletDC, please check that all devices
are\npowered and connected correctly, and that all fans are on.\nUse the help
command to view bench setup directions.\n\nPress [ANY KEY] when you are
ready.');
```

pause; clc;

```

%% Organize instrument information and communication
[inst,n] = instArchive;

% Setup instrument objects and clear previous settings
[eqp] = openGPIB(inst,n);

% Instrument index reference:
% 1. N9010A Signal Analyzer at 18
% 2. 33220A Signal Generator at 10 (BOP control)
% 3. N5181A Signal Generator at 19 (RF input)
% 4. Agilent MSO7104A Oscilloscope
sigAna = eqp(1).obj;
bopGen = eqp(2).obj;
rfGen = eqp(3).obj;
scope = eqp(4).obj;

%% Run test procedure
% Recall test states, configure instruments, and turn on generators
```

```

instConfig(sigAna,bopGen,scope,rfGen,eqp);

% Test measurement loop
[poutdBm,harmsdBm,pdissW,vData,iData] =
testProc(sigAna,bopGen,rfGen,scope);

% After performing all of the routine actions, close all instrument
objects
closeGPIB(eqp,n);

%% Data manipulation
% Calculate desired results from gathered data
[pindBm,pinW,poutW,eff,gain,thd] = hCalcs(poutdBm,harmsdBm,pdissW);

% Transpose results and group together for use with excel table format
poutW = poutW'; pindBm = pindBm'; pinW = pinW'; pdissW = pdissW'; eff =
eff';
gain = gain'; thd = thd'; vData = vData'; iData = iData';

% Create structured names for data for ease of use in MATLAB cmd window
i = 0;
for vDC = vDCMin:vDCStep:vDCMax
    i = i + 1;
    dcID = matlab.lang.makeValidName(sprintf('%dVDC',vDC));
    group.(dcID) =
[poutW(:,i),iData(:,i),gain(:,i),pdissW(:,i),eff(:,i),thd(:,i)];
end

end

function [obj,n] = instArchive
%% instArchive acts as a library of communication data for the
% instruments that will be used in the test

n = 0;

% 1. Agilent N9010A Signal Analyzer
n = n+1;
obj(n).name      = 'N9010A';
obj(n).type      = 'visa-gpib';
obj(n).mfg       = 'AGILENT';
obj(n).cnxn      = 'GPIB0';
obj(n).addr      = 18;
obj(n).visaAddr  = sprintf('%s::%d::0::INSTR',obj(n).cnxn,obj(n).addr);

% 2. Agilent 33220A Signal Generator 1 (LF mod)
n = n+1;
obj(n).name      = '33220A';
obj(n).type      = 'visa-gpib';
obj(n).mfg       = 'AGILENT';
obj(n).cnxn      = 'GPIB0';
obj(n).addr      = 10;
obj(n).visaAddr  = sprintf('%s::%d::0::INSTR',obj(n).cnxn,obj(n).addr);

% 3. Agilent N5181A Signal Generator
n = n+1;

```

```

obj(n).name      = '5181A';
obj(n).type      = 'visa-gpib';
obj(n).mfg       = 'AGILENT';
obj(n).cnxn      = 'GPIB0';
obj(n).addr      = 19;
obj(n).visaAddr  = sprintf('%s::%d::0::INSTR',obj(n).cnxn,obj(n).addr);

% 4. Agilent MS07104A Oscilloscope
n = n+1;
obj(n).name      = 'MS07104A';
obj(n).type      = 'visa-usb';
obj(n).mfg       = 'AGILENT';
obj(n).cnxn      = 'USB0';
obj(n).addr      = '0x0957::0x1755::my48260761';
obj(n).visaAddr  = sprintf('%s::%s::0::INSTR',obj(n).cnxn,obj(n).addr);

end

function [output] = openGPIB(input,num)
    %% openGPIB opens up the lines of communication between the test
    equipment and MATLAB

    for n = 1:num
        % Check existence of inst objects and create ones that don't exist
        output(n).obj = instrfind('Type',
input(n).type,'RsrcName',input(n).visaAddr,'Tag','');

        if isempty(output(n).obj)
            output(n).obj = visa(input(n).mfg,input(n).visaAddr);
        else
            fclose(output(n).obj);
        end

        fopen(output(n).obj);
        if n == num
            fprintf('Matlab has found connections with the following devices:
\n-----')
            output.obj
        end

        % Reset instrument states
        set(output(n).obj,'EOSMode','read&write')
        set(output(n).obj,'EOSCharCode','LF')
        fprintf(output(n).obj,'*CLS;*RST');
    end

end

function instConfig(sigAna,bopGen,scope,rfGen,eqp)
    %% instConfig prepares each instrument for the test by loading save
    % states, configuring various initial parameters, and turning on
    % instruments in proper order

    global rfFreq rfPwr warmTime bopDC

    fprintf('Initializing instruments, please stand by...\n');
    fprintf('Configuring instruments...');

```

```

% Initialize all equipment
anaInit(sigAna)
scopeInit(scope);
lfgenInit(bopGen,bopDC);
rfgenInit(rfGen,rfPwr,rfFreq);
fprintf(' check.\n');

% Turn on signal generators in this order:
% 1. VDS
% 2. RF Input
fprintf('Engaging signal generators...');
for n = 2:3
    fprintf(eqp(n).obj,'OUTP:STAT ON');
    pause(3)
end
fprintf(' check.\n');

% Warm up amplifier
fprintf('Warming up amplifier (%.2f seconds)...',warmTime)
warmUp(warmTime);
fprintf(' check.\n');

end

function anaInit(sigAna)
%% anaInit pulls up the prepared save state for the signal analyzer

    fprintf(sigAna,':MMEM:LOAD:STAT "Class H Pallet Amp Wideband sans
coupler.state"');

end

function scopeInit(scope)
%% scopeInit pulls up the prepared save state for the oscilloscope

    fprintf(scope,'RECALL:SETUP 2');

end

function lfgenInit(gen,dc)
%% lfgenInit configures the low frequency generator for use as a
% remote programming source for the BOP

    fprintf(gen,'*RCL 2');
    fprintf(gen,'FUNC DC');
    fprintf(gen,'VOLT:OFFS %d V',dc);

end

function rfgenInit(rfGen,rfPwr,rfFreq)
%% rfgenInit configures the high frequency generator for use as the
% RF input source for the device under test

    fprintf(rfGen,'POWER:AMPLitude %d::FREQUENCY:CW
%dMHZ',[rfPwr,rfFreq],'sync');

```



```

end

function warmUp(warmTime)
    %% warmUp halts all interactions with the device under test to allow
    %   for heat stabilization

    pause(warmTime);

end

function [poutdBm,harmsdBm,pdissW,vData,iData] =
testProc(sigAna,bopGen,rfGen,scope)
    %% testProc performs the actual measurement test procedure.
    %   The test itself consists of the following steps:
    %   1. Set DC rail voltage
    %   2. Set input power
    %   3. Measure amplifier output power and power consumption
    %   4. Repeat until all cases are satisfied

    %% Setup
    global vScale iScale cplErr warmTime mkrNum...
           vDCMin vDCStep vDCMax vDCSize...
           pinMin pinStep pinMax pinSize

    clc;

    % Preallocate data matrices and assign measurement counter sizes
    m = 0; n = 0;
    poutdBm = zeros(vDCSize,pinSize,mkrNum);
    pdissW   = zeros(vDCSize,pinSize);
    vData    = zeros(vDCSize,pinSize);
    iData    = zeros(vDCSize,pinSize);

    % Signal test start
    for beeper = 1:3
        fprintf(bopGen,'SYST:BEEP');
        pause(.25)
    end

    %% Perform test
    for VDS = vDCMin:vDCStep:vDCMax
        m = m+1;
        fprintf('Running test for VDS = %.2f V...',VDS);

        % Actual LF sig gen settings:
        bopDC = -VDS/vScale; %[V]
        fprintf(bopGen,'VOLT:OFFS %d V',bopDC);

        for Pin = pinMin:pinStep:pinMax
            n = n+1;
            % Set input power for RF gen
            fprintf(rfGen,'POW:AMPL %dDBM',Pin);

            % Give amp some time to warm up with each power setting
            warmUp(warmTime);

            % Grab output power

```

```

        for mkrCount = 1:mkrNum
            mkrCmd = sprintf('CALC:MARK%d:Y?',mkrCount);
            poutdBm(m,n,mkrCount) = str2num(query(sigAna,mkrCmd)) +
cplErr(mkrCount);
        end

        % Grab dissipated power
        fprintf(scope, 'MEAS:SOUR MATH');
        pdissW(m,n) = str2num(query(scope, 'MEAS:VRMS?'));

        % Grab voltage and current
        fprintf(scope, 'MEAS:SOUR CHAN1');
        vData(m,n) = str2num(query(scope, 'MEAS:VRMS?'));
        fprintf(scope, 'MEAS:SOUR CHAN2');
        iData(m,n) = str2num(query(scope, 'MEAS:VRMS?'));

    end
    n = 0;
    fprintf(' check.\n\n');

end

pdissW = pdissW.*vScale.*iScale;
vData = vData.*vScale;
iData = iData.*iScale;
harmsdBm = poutdBm(:, :, 2:mkrNum);
poutdBm = poutdBm(:, :, 1);

%% Conclude test
% Signal test completion
for beeper = 1:3
    fprintf(bopGen, 'SYST:BEEP');
    pause(.25)
end
clc;

end

function closeGPIO(eqp,n)
    %% closeGPIO closes channels of communication after the test is complete

    fprintf('Test complete. Disengaging signal generators...');
    for n = n:-1:1
        % If equip is a generator, shut off output first
        if n == 2 || n == 3
            % Shut off order:
            % 1. RF Input
            % 2. VDS AC
            fprintf(eqp(n).obj, 'OUTP:STAT OFF;');
            pause(3)
        end
        fclose(eqp(n).obj);
        delete(eqp(n).obj);
    end
    fprintf(' check.\n');

end

```

```

function [pindBm, pinW, poutW, eff, gain, thd] = hCalcs(poutdBm, harmsdBm, pdissW)
    %% hCalcs performs the calculations for efficiency and gain using the
    %   data gathered from testProc

    global pinMin pinStep pinMax preGain vDCSize

    %% Input power at input to Pallet amp itself
    pindBm = (pinMin:pinStep:pinMax) + preGain;

    %% Convert from dBm to watts
    pinW = repmat(dBmConv(pindBm, 'dBm'), vDCSize, 1);
    pindBm = dBmConv(pinW, 'w');
    poutW = dBmConv(poutdBm, 'dBm');
    harmsW = dBmConv(harmsdBm, 'dBm');

    %% Calculate efficiency, gain, thd
    eff = 100.*(poutW-pinW)./pdissW;
    gain = poutdBm - pindBm;

    % Sum the harmonics together by summing down the "z" (or 3rd) axis,
    % resulting in a 2D matrix that can be divided by poutW
    thd = 100.*sqrt(sum(harmsW, 3)./poutW);

end

function [out] = dBmConv(in, units)
    %% dBmConv performs the desired conversion from Watts to dBm and vice
    %   versa. Note that the "units" input is with respect the the input
    %   format, not the output format

    %% Input dBm, get Watts back
    if strcmpi(units, 'dBm')
        out = (10.^(in./10))./1000;
    end
    %% Input Watts, get dBm back
    if strcmpi(units, 'w')
        out = 10.*log10(in.*1000);
    end
end
end

```

## A.2 Live Efficiency Measurement Test Code

```
%% Written by Tom Larter
% This program records voltage, current, power, and efficiency data for a
% pallet amplifier while a LLRF test bench experiment is in progress.
%
% Bench setup:
%   LLRF:
%   - Connect a 80.5MHz, +10dBm signal source to the reference input
%   - Connect the RF drive output of the LLRF to the input of the power
%   amplifier
%   - Connect ethernet cable from network to LAN port on back
%   - Make sure that power connections to NIM crate are correct and
%   that the power is on
%
%   Scope:
%   - Ch 1 on BOP remote out voltage on LLRF box
%   - Ch 2 on BOP remote out current on LLRF box
%   - Ch 4 connected to Signal Analyzer trigger out on back of analyzer
%   - Uses save state "3"
%
%   Signal Analyzer:
%   - Connect 40dB coupler to input through 20dB attenuator
%   - Uses save state "RT EFF Class H Narrow Band Harmonics auto
cal.state"
%
%   BOP:
%   - Connect Dsub 9 connector to back of LLRF box
%   - Connect front panel output to PA with a banana-CPC cable
%   - Connect front panel negative output to ground
%
%   Power amp:
%   - Connect output to input of Narda output coupler
%
%   Narda Coupler:
%   - Connect output to input of Werlatone Coupler
%   - Connect reverse coupling to a 50 Ohm load
%   - Connect forward coupling to a 10dB passive attenuator
%
%   10dB Passive Attenuator:
%   - Connect output to RF input of variable attenuator
%
%   Variable Attenuator:
%   - Connect RF output to input of ZHL-1A preamp
%
%   LF Signal Generator:
%   - Connect output to variable attenuator CV input
%
%   Preamp:
%   - Connect output to LLRF feedback input
%   - Make sure that 24V connection is hooked up to terminal strip and
%   that the 24V PS is switched on (fan attached to underside of rack
%   mount should come on)
%
%   Werlatone Coupler:
%   - Connect output to 50 Ohm high power load
%   - Connect reverse coupling to a 50 Ohm load
```

```

%       - Connect forward coupling to the signal analyzer input
%
% LLRF Box settings:
% - Gain range switch set to "x5", BOP gain knob should be tuned so that
% a remote input of -5V results in a BOP output of 18V
% - MOD SEL should be flipped down so that the green "LLRF" indicator LED
% lights up
%
% Output syntax:
% [poutW,pindBm,pinW,pdissW,eff,gain,thd,vData,iData,group] = palletDC
%
% Written 12/17/2014

function [t,vs,is,psuppW,poutW,eff] = llrfEff
    %% House keeping
    clc; close all;

    % Check test readiness before running
    fprintf('Before running llrfEff, please check that all devices
are\npowered and connected correctly, and that all fans are on.\n\nPress
[ENTER] when you are ready. ');
    cd Functions; pause; clc;

    %% Organize instrument information and communication
    [inst,instNum] = instArchive;
    % Instrument index reference:
    % 1. N9010A Signal Analyzer at 18
    % 2. Agilent MSO7104A Oscilloscope at USB0 0761 address

    % Setup instrument objects and clear previous settings
    [eqp] = openGPIB(inst,instNum);

    % Attach ref. names to objects to make code more readable when able
    sigAna = eqp(1).obj;
    scope = eqp(2).obj;

    %% Run instrument test procedure
    % Initialize instruments
    anaInit(sigAna);
    scopeInit(scope);

    % Grab data
    [t,vs,is,psuppW,poutW,eff] = testProc(sigAna,scope);

end

function [obj,n] = instArchive
    %% instArchive acts as a library of communication data for the
    % instruments that will be used in the test

    n = 0;

    % 1. Agilent N9010A Signal Analyzer
    n = n+1;
    obj(n).name = 'N9010A';
    obj(n).type = 'visa-gpib';
    obj(n).mfg = 'AGILENT';
    obj(n).cnxn = 'GPIB0';

```

```

obj(n).addr      = 18;
obj(n).visaAddr = sprintf('%s::%d::0::INSTR',obj(n).cnxn,obj(n).addr);

% 2. Agilent MSO7104A Oscilloscope
n = n+1;
obj(n).name      = 'MSO7104A';
obj(n).type      = 'visa-usb';
obj(n).mfg       = 'AGILENT';
obj(n).cnxn      = 'USB0';
obj(n).addr      = '0x0957::0x1755::my48260761';
obj(n).visaAddr = sprintf('%s::%s::0::INSTR',obj(n).cnxn,obj(n).addr);

end

function [output] = openGPIB(input,num)
    %% openGPIB opens up the lines of communication between the test
    equipment and MATLAB

    for n = 1:num
        % Check existence of inst objects and create ones that don't exist
        output(n).obj = instrfind('Type',
input(n).type,'RsrcName',input(n).visaAddr,'Tag','');

        if isempty(output(n).obj)
            output(n).obj = visa(input(n).mfg,input(n).visaAddr);
        %#ok<TNMLP,*AGROW>
        else
            fclose(output(n).obj);
        end

        fopen(output(n).obj);
        if n == num
            fprintf('Matlab has found connections with the following devices:
\n-----')
            output.obj
        end

        % Reset instrument states
        set(output(n).obj,'EOSMode','read&write')
        set(output(n).obj,'EOSCharCode','LF')
        fprintf(output(n).obj,'*CLS;*RST');
        set(output(n).obj,'Timeout',100);

    end
end

function anaInit(sigAna)
    %% anaInit pulls up the prepared save state for the signal analyzer

    fprintf(sigAna,':MMEM:LOAD:STAT "RT EFF Class H Narrow Band Harmonics
auto cal.state"');
    fprintf(sigAna,':INIT:CONT ON');

end

function scopeInit(scope)
    %% scopeInit pulls up the prepared save state for the oscilloscope

```

```

fprintf(scope, 'RECALL:SETUP 3');

end

function [t,vs,is,psuppW,poutW,eff] = testProc(sigAna,scope)
%% testProc performs the actual measurement test procedure.
% The test itself consists of the following steps:
% 1. Measure supplied voltage and current
% 2. Measure output power from the power amplifier
% 3. Calculate output wattage and efficiency based on measurements
% 4. Plot results to a constantly-updating figure

%% Setup
vScale = 3.6;
iScale = 1.2;
dataPts = 100;

blank = zeros(1,dataPts);
t = blank; vs = blank; is = blank; podBm = blank;
psuppW = blank; poutW = blank; eff = blank;

%% Test procedure
fprintf('\nGrabbing data... \n')
tstart = tic;
for i = 1:dataPts
    % Mark time of measurement
    t(i) = toc(tstart);

    % Measure voltage and current and calculate dissipated power
    fprintf(scope, 'MEAS:SOUR CHAN1');
    vs(i) = vScale*str2double(query(scope, 'meas:vav?'));
    fprintf(scope, 'MEAS:SOUR CHAN2');
    is(i) = iScale*str2double(query(scope, 'meas:vav?'));

    % Measure output power
    podBm(i) = str2double(query(sigAna, 'calc:mark1:y?'));

    % Calculate output wattage and efficiency
    psuppW(i) = vs(i)*is(i);
    poutW(i) = 10^((podBm(i)-30)/10);
    eff(i) = 100*poutW(i)/psuppW(i);

    % Print data in legend
    legend(sprintf('V_r_a_i_l: %.2fV P_O_u_t: %.2fW Eff:
%.2f%%', vs,poutW,eff(i)));

    % Draw data in plot
    if i > 2
        xlim([t(2), t(length(t))]);
        refreshdata(h, 'caller');
        drawnow
    end
end
end

```

## **BIBLIOGRAPHY**



## BIBLIOGRAPHY

- [1] T. Glasmacher, "FRIB Groundbreaking Launches Civil Construction," 17 March 2014. [Online]. Available: <http://www.frib.msu.edu/content/frib-groundbreaking-launches-civil-construction>.
- [2] "FRIB Construction Site Cameras," Erdman Video Systems, [Online]. Available: <http://video-monitoring.com/construction/msufrib/index.htm>.
- [3] FRIB, "About FRIB," 2014. [Online]. Available: <http://frib.msu.edu/about>. [Accessed 8 November 2014].
- [4] H. Krauss, C. Bostian and F. Raab, *Solid State Radio Engineering*, New York: John Wiley & Sons, 1980, pp. 519-520.
- [5] M. Kazimierczuk, *RF Power Amplifiers*, New York: John Wiley & Sons, 2008, pp. 331-332.
- [6] P. Lavrador, T. Cunha, P. Cabral and J. Pedro, "The Linearity-Efficiency Compromise," *IEEE Microwave Magazine*, vol. 11, pp. 44-58, Aug. 2010.
- [7] F. Raab, P. Asbeck, S. Cripps, P. Kenington, Z. Popovich, N. Pothecary, J. Sevic and N. Sokal, "RF and Microwave Power Amplifier and Transmitter Technologies - Part 3," *High Frequency Design*, vol. 2, pp. 34-48, 2003.
- [8] A. Saleh and D. Cox, "Improving the Power-Added Efficiency of FET Amplifiers Operating with Varying-Envelope Signals," *IEEE Transactions on Microwave Theory and Techniques*, vol. 31, no. 1, pp. 51-56, 1983.
- [9] B. Geller, F. Assal, R. Gupta and P. Cline, "A Technique for the Maintenance of FET Power Amplifier Efficiency Under Backoff," *IEEE MTT-S Microwave Symposium Digest*, vol. 3, pp. 949-952, 1989.
- [10] D. Kimball, J. Yan, P. Theilmann, M. Hassan, P. Asbeck and L. Larson, "Efficient and Wideband Envelope Amplifiers for Envelope Tracking and Polar Transmitters," in *Power Amplifiers and Radio Applications (PAWR), IEEE Topical Conference on*, Santa Clara, CA, 2013.
- [11] P. Draxler, S. Lanfranco, D. Kimball, C. Hsia, J. Jeong, J. van de Sluis and P. Asbeck, "High Efficiency Envelope Tracking LDMOS Power Amplifier for W-CDMA," in *IEEE Microwave Symposium Digest*, San Francisco, CA, 2006.
- [12] R. Wu, Y. Liu, J. Lopez, C. Schecht, Y. Li and D. Lie, "High-Efficiency Silicon-Based Envelope-Tracking Power Amplifier Design With Envelope Shaping for Broadband Wireless Applications," *Solid-State Circuits, IEEE Journal of*, vol. 48, no. 9, pp. 2030-2040, 2013.
- [13] G. Wimpenny, J. Hildersley, T. Vlasits, S. Cummins and N. Padfield, "Envelope Tracking GaAs HBT PA Performance Characterization Under High Load Mismatch Conditions," in *Power Amplifiers for Wireless and Radio Applications (PAWR), IEEE Topical Conference on*, Santa Clara, CA, 2012.

- [14] G. Wimpenny, "Understand and characterize envelope-tracking power amplifiers," *EE Times*, [Online]. Available: [http://www.eetimes.com/document.asp?doc\\_id=1279313](http://www.eetimes.com/document.asp?doc_id=1279313). [Accessed 13 November 2014].
- [15] J. Jeong, D. Kimball, M. Kwak, C. Hsia, P. Draxler and P. Asbeck, "Wideband Envelope Tracking Power Amplifiers with Reduced Bandwidth Power Supply Waveforms and Adaptive Digital Predistortion Techniques," *Microwave Theory and Techniques, IEEE Transactions on*, vol. 57, no. 12, pp. 3307-3314, 2009.
- [16] B. Minnis, P. Moore, P. Blanken and M. van der Heijden, "System-Efficiency Analysis of Power Amplifier Supply-Tracking Regimes in Mobile Transmitters," *Circuits and Systems, IEEE Transactions on*, vol. 56, no. 1, pp. 268-279, 2009.
- [17] C. Hsia, D. Kimball, S. Lanfranco and P. Asbeck, "Wideband High Efficiency Digitally-Assisted Envelope Amplifier with Dual Switching Stages for Radio Base-Station Envelope Tracking Power Amplifiers," in *IEEE Microwave Symposium Digest*, Anaheim, CA, 2010.
- [18] S. Modi, P. Balsara and O. Eliezer, "Reduced Bandwidth Class H Supply Modulation for Wideband RF Power Amplifiers," in *IEEE Wireless and Microwave Technology Conference*, Cocoa Beach, FL, 2012.
- [19] S. Modi, S. Kanigere, O. Eliezer and P. Balsara, "A Limited Bandwidth Envelope Follower for Efficiency Enhancement in a Linear Power Amplifier in Broadband Transmitters," in *IEEE Circuits and Systems Workshop: System-on-Chip - Design, Applications, Integration, and Software*, Dallas, TX, 2008.
- [20] Z. Wang, R. Ma, X. Yang and S. Lanfranco, "Driver Amplifier Design Considerations for High Efficiency Envelope Tracking Power Amplifier Line-Up," in *Wireless and Microwave Technology Conference (WAMICON), IEEE*, Cocoa Beach, FL, 2012.
- [21] D. Kimball, J. Jeong, C. Hsia, P. Draxler, S. Lanfranco, W. Nagy, K. Linthicum, L. Larson and P. Asbeck, "High-Efficiency Envelope-Tracking W-CDMA Base-Station Amplifier Using GaN HFETs," *Microwave Theory and Techniques, IEEE Transactions on*, vol. 54, no. 11, pp. 3848-3856, 2006.
- [22] C. Yu and A. Zhu, "A Single Envelope Modulator-Based Envelope-Tracking Structure for Multiple-Input and Multiple-Output Wireless Transmitters," *Microwave Theory and Techniques, IEEE Transactions on*, vol. 60, no. 10, pp. 3317-3327, 2012.
- [23] P. Gilabert and G. Montoro, "Look-Up Table Implementatino of a Slow Envelope Dependent Digital Predistorter for Envelope Tracking Power Amplifiers," *IEEE Microwave and Wireless Components Letters*, vol. 22, no. 2, pp. 97-99, 2012.
- [24] Broadcast Concepts, "55-88MHz 12W Band I VHF TV Driver," [Online]. Available: <http://broadcastconcepts.com/VHFTV-15L.html>. [Accessed 11 November 2014].

- [25] S. Zhao, *Practical Solutions to the Non-Minimum Phase and Vibration Problems Under the Disturbance Rejection Paradigm*, Ph.D. dissertation, Cleveland: Cleveland State Univ., 2012.
- [26] Z. Zheng, Z. Liu, J. Wei, S. Zhao and Y. Zhang, "ADRC Control for Beam Loading and Microphonics," in *LINAC2012*, Tel-Aviv, Israel, 2012.
- [27] A. N. Laboratory, "Experimental Physics and Industrial Control System (EPICS)," Argonne National Laboratory, [Online]. Available: [www.aps.anl.gov/epics/](http://www.aps.anl.gov/epics/). [Accessed 12 March 2015].
- [28] H. M. GmbH, "Main page," 2015. [Online]. Available: <http://www.hbhmw.de/>. [Accessed 22 April 2015].